molecular pharmaceutics

pubs.acs.org/molecularpharmaceutics

Article

Development and Validation of Novel Z-360-Based Macromolecules for the Active Targeting of CCK2-R

Elisa Vettorato,◆ Marco Verona,◆ Greta Bellio, Stefania Croci, Riccardo Filadi, Alessandra Bisio, Eugenia Spessot, Alberto Andrighetto, Devid Maniglio, Mattia Asti, Giovanni Marzaro,* and Francesca Mastrotto*

Cite This: *Mol. Pharmaceutics* 2024, 21, 3848−3865

Read Online

ACCESS | Metrics & More | Article Recommendations | Supporting Information

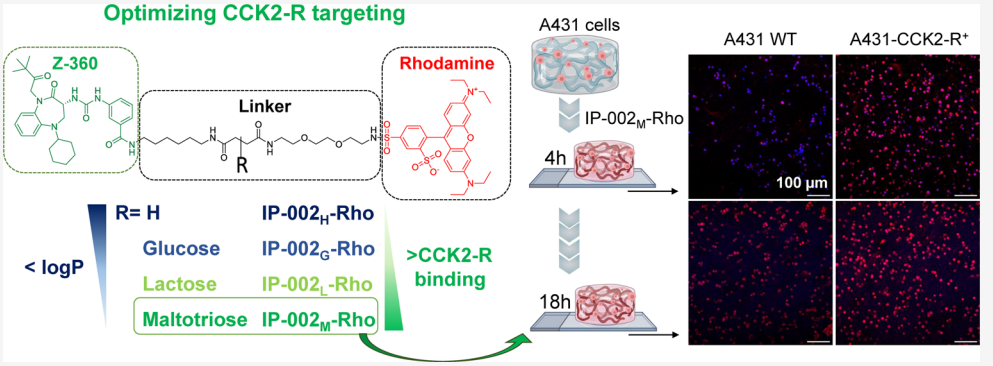

ABSTRACT: The cholecystokinin type 2 receptor (CCK2-R) represents an ideal target for cancer therapy since it is overexpressed in several tumors and is associated with poor prognosis. Nastorazepide (Z-360), a selective CCK2-R antagonist, has been widely investigated as a CCK2-R ligand for targeted therapy; however, its high hydrophobicity may represent a limit to cell selectivity and optimal in vivo biodistribution. Here, we present three new fluorescent Z-360 derivatives (**IP-002$_G$-Rho, IP-002$_L$-Rho, and IP-002$_M$-Rho**) in which nastorazepide was linked, through spacers bearing different saccharides (glucose (G), lactose (L), and maltotriose (M)), to sulforhodamine B. A fourth compound (**IP-002$_H$-Rho**) with no pendant sugar was also synthesized as a control. Through two-dimensional (2D) and three-dimensional (3D) in vitro studies, we evaluated the compound association with and selectivity for CCK2-R-overexpressing cells (A431-CCK2-R$^+$) vs CCK2-R-underexpressing cells (A431 WT). 2D in vitro studies highlighted a progressive increase of IP-002$_x$-Rho association with A431-CCK2-R$^+$ cells according to the linker hydrophilicity, that is, maltotriose > lactose > glucose > hydrogen, with **IP-002$_M$-Rho** showing a 2.4- and a 1.36-fold higher uptake than **IP-002$_G$-Rho** and **IP-002$_L$-Rho**, respectively. Unexpectedly, **IP-002$_H$-Rho** showed a similar cell association to that of **IP-002$_L$-Rho** but with no difference between the two tested cell lines. On the contrary, association with A431-CCK2-R$^+$ cells as compared to the A431 WT was found to be 1.08-, 1.14-, and 1.37-fold higher for **IP-002$_G$-Rho**, **IP-002$_L$-Rho**, and **IP-002$_M$-Rho**, respectively, proving **IP-002$_M$-Rho** to be the best-performing compound, as also confirmed by competition studies. Trafficking studies on A431-CCK2-R$^+$ cells incubated with **IP-002$_M$-Rho** suggested the coexistence of receptor-mediated endocytosis and simple diffusion. On the contrary, a high and selective uptake of **IP-002$_M$-Rho** by A431-CCK2-R$^+$ cells only was observed on 3D scaffolds embedded with cells, underlining the importance of 3D models in in vitro preliminary evaluation.

KEYWORDS: *CCK2-R, nastorazepide, cancer, in vitro 3D model, targeted therapy*

1. INTRODUCTION

The cholecystokinin type 2 receptor (CCK2-R, known before as CCKB or gastrin receptor) has been regarded as a relevant therapeutic target since the discovery of its high expression in malignant tissues in the 1960s.[1] Gastrin receptors contribute to neoplastic transformations, and high levels of CCK2-R have been observed in gastric, pancreatic, colorectal, esophageal, and several other types of cancer.[2] Its overexpression is generally correlated with cell proliferative phenomena and poor prognosis of the patients.[3−8] CCK2-R is an attractive target to mediate the accumulation of diagnostic or therapeutic radionuclides at the tumor site by surface modification of specific carriers with various CCK2-R ligands. Active targeting

Received: February 4, 2024
Revised: June 25, 2024
Accepted: June 25, 2024
Published: July 3, 2024

Scheme 1. Synthesis of the Derivatizable Fluorescent Intermediate 8. ***Reagents and Conditions*****: (a) N-Boc-1,6-hexandiamine, EDC·HCl, TEA, DMAP, CH_2Cl_2, Room Temperature, 16 h, and 90% Yield, (b) TFA, CH_2Cl_2, Room Temperature, 1 h, and Quantitative Yield, (c) Maleic Anhydride, MeCN, Room Temperature, 16 h, and 94% Yield, (d) HATU, TEA, DMF, Room Temperature, 16 h, and 61% Yield, (e) TFA, CH_2Cl_2, Room Temperature, 1 h, and Quantitative Yield, and (f) Rhodamine B Sulfonyl Chloride TEA, DMF, Room Temperature, 16 h, and 73% Yield**

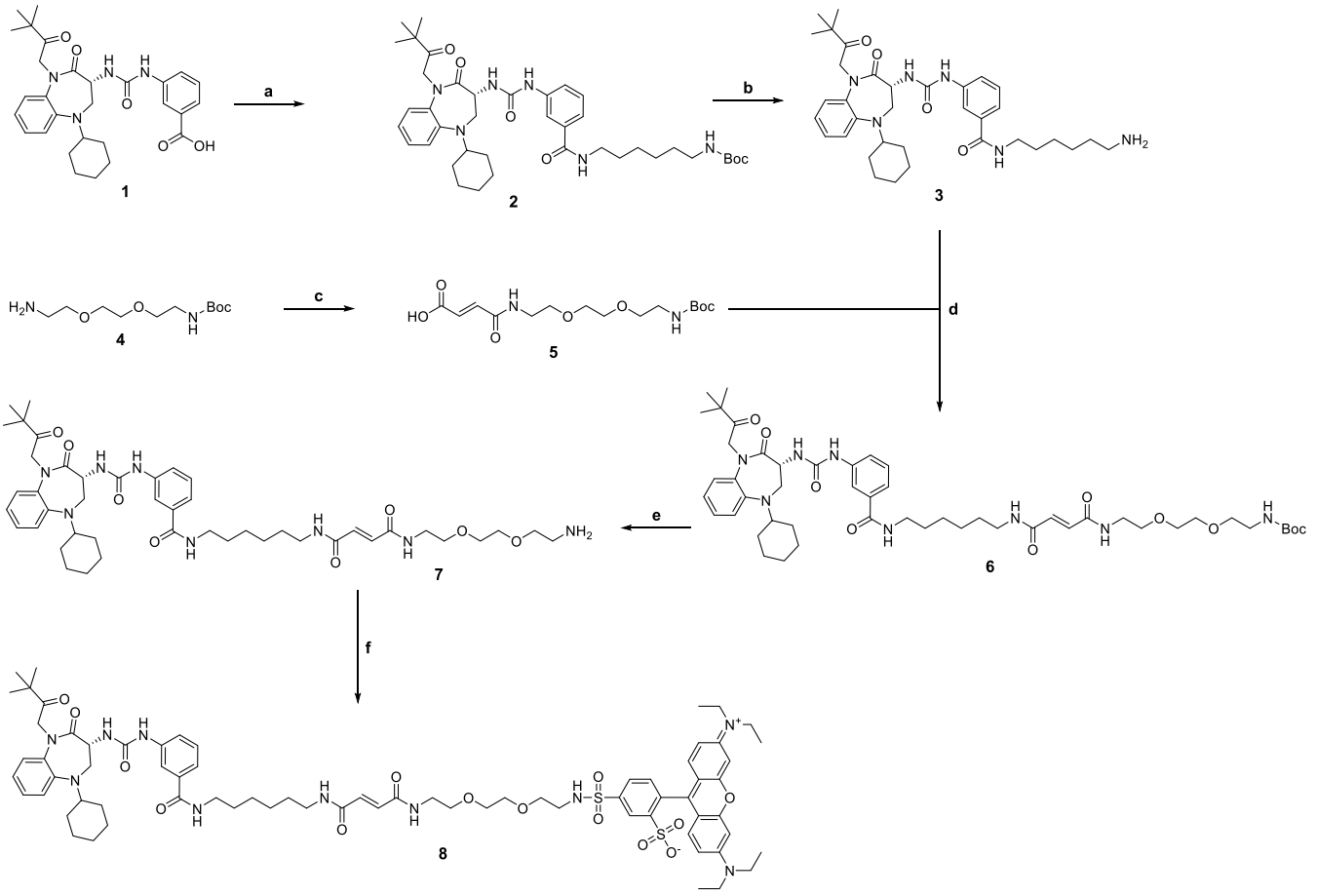

of tumors based on targeting moieties such as ligands and antibodies has been efficiently exploited for the delivery of therapeutic radionuclides, opening the path for the use of radioimmunoconjugates[9−11] (RIT) or peptide receptor radiotherapy[12,13] (PRRT) in the clinic. This led to several FDA- and EMA-approved radiopharmaceuticals (e.g.,^{90}Y-Ibritumomab tiuxetan,[14] ^{177}Lu-oxodotreotide,[15] and the recent ^{177}Lu-PSMA-617[16]).[17,18] In particular, the delivery of radionuclides with small molecules could be beneficial to achieve quick distribution and accumulation of the drug in the tumor site in vivo, avoiding drawbacks such as immunogenicity, low stability or shelf life, or high production costs of antibody-based drug delivery systems.[19] For example, the group of Wild designed ^{177}Lu-PP-F11N, a minigastrin analogue linked through 6 units of D-glucose to a DOTA chelator labeled with ^{177}Lu (^{177}Lu-DOTA-(D-Glu)$_6$-Ala-Tyr-Gly-Trp-Nle-Asp-PheNH$_2$) for the radionuclide therapy of medullary thyroid carcinoma.[20] A phase 0 study showed low toxicity and tumor accumulation of this compound in all patients, and an early phase I clinical trial in combination or not with the neprilysin inhibitor sacubitril was recently completed (NCT03647657). Being inspired by natural ligands, over the years, a variety of minigastrin (MG)- and cholecystokinin (CCK)-targeting radiopeptides were developed and screened at a preclinical level.[21] Major limitations to their further progress into the clinic concern kidney accumulation and rapid enzymatic degradation after in vivo administration. Moreover, radiopeptides generally act as CCK2-R agonists, leading to similar side effects to those produced, for example, by pentagastrin, like nausea and abdominal cramping.[22] This paved the way for the investigation of nonpeptide antagonists, initially screened as therapeutics. A fair number of nonpeptide CCK2-R-antagonists have been developed, and two benzodiazepine derivatives, netazepide (YF460) and nastorazepide (Z-360, compound in Scheme 1), reached phase II clinical trials as promising anticancer drugs. Despite that, the lack of a clear and significant improvement in the patient outcomes with the use of those molecules over the standard therapies prevented their entrance into the clinic.[23] Although these molecules did not succeed as therapeutic drugs and are not supposed to be internalized by cells, they are highly valuable targeting agents, especially when new macromolecules are designed for targeted radiotherapy. Indeed, in comparison to the cognate peptide agonist, they showed better stability and pharmacokinetic profiles and, importantly, better tumor localization.[24−26] Among all of the nonpeptide agonists, nastorazepide is of particular interest due to the presence of a functional carboxylic group not involved in the binding to the receptor, which is available for further modification.

https://doi.org/10.1021/acs.molpharmaceut.4c00124
Mol. Pharmaceutics 2024, 21, 3848−3865

In our previous work, **IP-001**, a novel nastorazepide-based SPECT tracer, was developed and showed promising in vivo stability and distribution; however, the remarkable hydrophobicity conferred to the macromolecules by Z-360 posed a limit to its tumor accumulation.[27] This observation was further supported by the unspecific binding phenomena registered with other lipophilic macromolecular systems[26,28] and suggested that increasing the hydrophilicity of macromolecules by modifying the linker between Z-360 and the selected chelator might be a successful approach. The use of polyethylene glycol is a common strategy to confer hydrophilicity to a molecule, but the recent discovery of PEG immunogenicity-related issues drove us to a different pathway.[29] Thus, we synthesized a small library of **IP-001** fluorescent analogues named **IP-002** and introduced pendant groups characterized by increasing hydrophilicity in the spacer, specifically a monosaccharide (glucose, G), a disaccharide (lactose, L), and a trisaccharide (maltotriose, M). The new linker was designed to improve the solubility of the molecules and, consequently, the selective interaction with CCK2-R-expressing cells by limiting its accumulation by passive diffusion. To confirm our hypothesis, we replaced the chelator with sulforhodamine B, which allows us to monitor in vitro the association of macromolecules with the human epidermoid squamous carcinoma cell wild type (A431 WT, not expressing the receptor) and transfected to express CCK2-R (A431-CCK2-R$^+$). Three-dimensional (3D) cellular models based on cells embedded in methacryloyl gelatin (GelMA)[30] scaffolds were also employed to compensate, at least partially, for the lack of complexity found in living tissues, well known to impair the adequate assessment of the drug behavior over time.[31]

2. MATERIALS AND METHODS

2.1. Materials. All chemicals of reagent grade were purchased from Fischer Scientific (Fisher Scientific Italia, Milan, Italy), Merck Life Science S.r.l. (Milan, Italy), and Iris Biotech GmbH (Marktredwitz, Germany) and were used without further purification unless otherwise specified. Solvents of analytical grade were obtained from Carlo Erba (Milan, Italy) or Lab Scan (Bangkok, Thailand) and degassed by ultrasonication for 15−20 min before use. Deuterated solvents for nuclear magnetic resonance (NMR) analysis exhibited an isotopic purity of 99.5% and were supplied by SG Isotec (Panevo, Republic of Serbia). All reaction intermediates were purified as specified in the following procedures, and their purity was ≥95% as assessed by NMR and/or high-resolution mass spectrometry (HRMS).

Dulbecco's modified Eagle medium (DMEM), L-glutamine solution, fetal bovine serum (FBS), penicillin−streptomycin solution, trypsin-EDTA solution, phosphate-buffered saline (PBS) with and without $CaCl_2$ and $MgCl_2$, ethylenediaminetetraacetic acid (EDTA), sodium azide, paraformaldehyde (PFA), Hoechst 33258, and Triton X-100 were supplied by Merck Life Science S.r.l (Milan, Italy). "Ultrapure" water (18.2 MΩ, Milli-Q grade) for the preparation of all suspensions and solutions was produced with a Millipore Milli-Q purification system (MA). Geneticin sulfate (G-418S), 4′,6-diamidino-2-phenylindole dihydrochloride (DAPI, Invitrogen), calcein, and bovine serum albumin (BSA) microbiological-grade powder were purchased from Fisher Scientific (Fisher Scientific Italia, Milan, Italy). Fura-2/AM was purchased from Abcam (Cambridge, U.K.). The ProLong Glass AntiFade mountant, rabbit antihuman EEA1 monoclonal antibody, and goat antirabbit IgG (H + L) cross-adsorbed secondary antibody conjugated with Alexa Fluor 488 were purchased from Thermo Fisher Scientific (Waltham, MA). Cholecystokinin octapeptide (CCK-8) unconjugated or conjugated with 6-carboxyfluorescein (6-FAM) at the *N*-terminus, CCK-8 (FAM), and gastrin I were custom-made by GenScript (Piscataway, New Jersey). Lithium phenyl-2,4,6-trimethylbenzoylphosphinate (LAP, > 98.0% (T) (HPLC)) was purchased from TCI Chemicals (TCI Europe, Switzerland). Propidium iodide and Oregon Green 488 phalloidin were obtained from Molecular Probes (Eugene, OR).

2.2. Instrumentation. NMR spectra were recorded on a Bruker 400-AMX spectrometer, using tetramethylsilane (TMS) as the internal standard. Mass spectrometry was performed on an Applied Biosystem Mariner System 5220 equipped with a MALDI TOF/TOF 400 Plus AB Sciex (Framingham, MA) analyzer. The purification of the synthesized compounds was carried out by an Interchim puriflash 5.125 preparative HPLC instrument equipped with a binary pump and UV−visible detector. A preparative Zorbax-Eclipse (Agilent) (C18; 5 μm; 150 mm × 21.2 mm) column was used. Eluents were H_2O + 0.1% TFA (A) and MeCN (B) at a flow of 1.7 mL/min in gradient mode from 10 to 100% eluent B in 28 min. The detection of reaction products was performed by evaluating the absorbance at λ = 254 and 565 nm. HPLC analyses for the solubility tests were performed on an RP-HPLC PU-2080 Plus (Jasco, Carpi, Italy) chromatographic system equipped with FP-2020 Plus and UV-2075 Plus detectors and a Luna C-18 column with 5 μm diameter, 250 mm × 460 mm size, and a porosity of 100 Å. Elution was performed using H_2O + 0.05% TFA (A) and MeCN + 0.05% TFA (B) as eluents with a gradient from 10% to 90% of eluent B in 30 min at a flow of 1 mL/min. The detection was performed at λ_{exc} = 553 nm and λ_{em} = 580 nm, with a 10× signal gain.

2.3. Synthesis of the Fluorescent Precursor IP-002$_x$-Rho. *2.3.1. Synthesis of Z-360-Hex-NH$_2$ (8). Synthesis of Z-360 (1).* The compound was synthesized as previously reported.[32]

Synthesis of Z-360-Hex-NH-Boc (2). To a solution of **1** (Z-360) (100 mg, 0.2 mmol) in CH_2Cl_2 (1 mL), *N*-Boc-1,6-hexandiamine (46.0 mg, 0.2 mmol), EDC·HCl (40.5 mg, 0.2 mmol), TEA (23.3 mg, 0.2 mmol), and 4-dimethylaminopyridine (25.8 mg, 0.2 mmol) were added. The reaction mixture was stirred for 16 h, and the progression was monitored by thin-layer chromatography (TLC) using $CHCl_3$/MeOH 9:1 as an eluent. Then, the reaction mixture was diluted in CH_2Cl_2 (10 mL) and washed with a saturated NH_4Cl solution (2 mL × 15 mL). The organic layer was dried over anhydrous Na_2SO_4, filtered, and concentrated under vacuum to yield **Z-360-Hex-NH-Boc** (**2**; 124.0 mg, 0.2 mmol, 90% yield).

^{1}H NMR (400 MHz, $CDCl_3$): δ 7.61 (s, 1H); 7.35 (d, J = 7.8 Hz, 1H); 7.26−7.20 (m, 2H); 7.14−7.04 (m, 2H); 7.03−6.95 (m, 2H); 6.66−6.61 (m, 1H); 5.34−5.25 (m, 1H); 4.82−4.73 (m, 1H); 4.71−4.59 (s, 1H); 4.58−4.47 (s, 1H); 4.19−4.07 (m, 1H), 3.40−3.30 (m, 4H); 3.09−3.05 (m, 2H); 2.15−2.02 (m, 1H); 1.90−1.79 (m, 4H); 1.78−1.71 (m, 6H); 1.63−1.56 (m, 4H); 1.45−1.41 (s, 9H); 1.28−1.18 (m, 4H); 1.16−1.12 (s, 9H).

Synthesis of Z-360-Hex-NH$_2$ (3). A solution of **2** (144.0 mg, 0.2 mmol) in CH_2Cl_2 (3 mL) was cooled to 0 °C, and then, trifluoroacetic acid (0.9 mL) was added dropwise. The reaction mixture was warmed to room temperature and stirred for 1 h

https://doi.org/10.1021/acs.molpharmaceut.4c00124
Mol. Pharmaceutics 2024, 21, 3848−3865

(TLC: $CHCl_3$/MeOH 9:1). The reaction mixture was concentrated under reduced pressure to yield **Z-360-Hex-NH$_2$** (**3**; 124.0 mg, 0.2 mmol, quantitative yield).

^{1}H NMR (400 MHz, $CDCl_3$): δ 7.80−7.71 (s, 1H); 7.44−7.30 (m, 3H); 7.26−7.16 (m, 2H); 7.10−7.01 (m, 2H); 5.25−5.17 (m, 1H); 4.70−4.63 (m, 1H); 4.30−4.23 (m, 1H); 3.50−3.30 (m, 4H); 3.10−3.00 (m, 2H); 2.12−2.00 (m, 1H); 1.90−1.80 (m, 4H); 1.75−1.50 (m, 10H); 1.33−1.24 (m, 4H); 1.16−1.13 (s, 9H).

*Synthesis of N-Boc-N′-(3-carboxyprop-2-en-1-only)-2,2′-(ethylenedioxy)diethylamine (**5**).* Maleic anhydride (0.4 g, 4.4 mmol) was added to a solution of *N*-Boc-2,2′-(ethylenedioxy)-diethylamine (**4**; 1.1 g, 4.4 mmol) in MeCN (25 mL). The reaction mixture was stirred for 16 h (TLC: $CHCl_3$/MeOH 9:1). At completion of the reaction, the organic solvent was evaporated under reduced pressure to yield ***N*-Boc-*N*′-(3-carboxyprop-2-en-1-only)-2,2′-(ethylenedioxy)diethylamine** (**5**; 1.4 g, 4.1 mmol, 94% yield).

^{1}H NMR (400 MHz, DMSO-d_6): δ 9.34 (s, 1H); 6.80−6.72 (m, 1H) 6.40−6.35 (d, J = 12.3 Hz, 1H); 6.25−6.21 (d, J = 12.4 Hz, 1H); 3.56−3.47 (m, 6H); 3.39−3.31 (m, 4H); 3.08−3.02 (m, 2H); 1.39 (s, 9H).

*Synthesis of Z-360-Hex-Link-NH_Boc (**6**).* *Compound* **5** (126.0 mg, 0.4 mmol) was dissolved in DMF (2 mL) followed by the addition of **3** (224.1 mg, 0.4 mmol), HATU (153.0 mg, 0.4 mmol), and TEA (79.9 mg, 0.8 mmol). The reaction mixture was stirred for 16 h at room temperature (TLC: $CHCl_3$/MeOH 9:1), diluted with EtOAc (10 mL), and washed with a brine solution (2 × 10 mL). The organic layer was dried over anhydrous Na_2SO_4, filtered, and concentrated under vacuum. The residue was purified by flash chromatography ($CHCl_3$/MeOH 9:1), to yield **Z-360-Hex-Link-NH-Boc** (**6**; 211.0 mg, 0.2 mmol, 61% yield).

^{1}H NMR (400 MHz, $CDCl_3$): δ 7.96 (s, 1H); 7.49−7.38 (m, 1H); 7.25−7.17 (m, 2H); 7.12−7.02 (m, 2H); 6.99−6.93 (m, 2H); 6.72−6.66 (m, 1H); 6.58−6.48 (m, 1H); 5.28−5.19 (m, 1H); 4.76−4.67 (m, 1H); 4.18−4.08 (m, 1H); 3.79−3.68 (m, 2H); 3.62−3.58 (m, 4H); 3.55−3.52 (m, 4H); 3.41−3.33 (m, 4H); 3.30−3.25 (m, 4H); 2.09−2.00 (m, 1H); 1.85−1.52 (m, 14H); 1.43 (s, 9H); 1.29−1.20 (m, 4H); 1.17 (s, 9H).

*Synthesis of Z-360-Hex-Link-NH$_2$ (**7**).* *Compound* **6** (78.6 mg, 83.0 μmol) was dissolved in CH_2Cl_2 (3 mL) and cooled to 0 °C. Then, TFA (0.9 mL) was added dropwise. The reaction mixture was warmed to room temperature and stirred for 1 h (TLC: $CHCl_3$/MeOH 9:1). The reaction mixture was concentrated under reduced pressure to yield **Z-360-Hex-Link-NH$_2$** (7; 68.0 mg, 83.0 μmol, quantitative yield).

^{1}H NMR (400 MHz, $CDCl_3$): δ 7.80 (s, 1H); 7.45−7.34 (m, 3H); 7.25−7.17 (m, 2H); 7.09−6.96 (m, 2H); 6.72−6.66 (m, 1H); 6.58−6.48 (m, 1H); 5.29−5.19 (m, 1H); 4.74−4.67 (m, 1H); 4.20−4.09 (m, 1H); 3.79−3.68 (m, 2H); 3.64−3.58 (m, 4H); 3.55−3.51 (m, 4H); 3.41−3.33 (m, 4H); 3.30−3.25 (m, 4H); 2.05−2.00 (m, 1H); 1.85−1.52 (m, 14H); 1.29−1.20 (m, 4H); 1.17 (s, 9H).

*Synthesis of Z-360-Hex-Link-Rho (**8**).* To a solution of **7** (31.9 mg, 23.0 μmol) in DMF (0.6 mL) were added rhodamine B sulfonyl chloride (8.7 mg, 15.0 μmol) and TEA (36.4 mg, 360.0 μmol). The reaction mixture was stirred for 16 h at room temperature (TLC: $CHCl_3$/MeOH 9:1). The reaction mixture was diluted with EtOAc (10 mL) and washed with a saturated NH_4Cl solution (2 mL × 10 mL). The organic layer was dried over anhydrous Na_2SO_4, then filtered, and concentrated under vacuum to yield **Z-360-Hex-Link-Rho** (**8**; 15.3 mg, 16.8 μmol, 73% yield).

^{1}H NMR (400 MHz, $CDCl_3$): δ 9.95 (bs, 1H); 8.83 (d, J = 1.6 Hz, 1H); 8.43 (bs, 1H); 8.05−7.97 (d, J = 8.3 Hz, 1H); 7.91−7.85 (d, J = 8.3 Hz, 1H); 7.55−7.50 (d, J = 7.7 Hz, 1H); 7.20−7.10 (m, 6H); 7.30−6.90 (m, 4H); 6.83−6.77 (m, 2H); 6.72−6.67 (m, 1H); 6.58−6.50 (m, 1H); 6.46 (d, J = 1.8 Hz, 1H); 6.42−6.34 (m, 1H); 6.00 (d, J = 2.2 Hz, 1H); 5.71−5.67 (d, J = 7.8 Hz, 1H); 5.25−5.20 (d, J = 17.9 Hz, 1H); 4.62−4.55 (m, 1H); 3.96−3.85 (m, 2H); 3.85−3.80 (d, J = 17.9 Hz, 1H); 3.70−3.10 (m, 24H); 2.54−2.46 (m, 1H); 2.13−2.02 (m, 2H); 2.00−1.92 (m, 1H); 1.82−1.76 (m, 1H); 1.70, 1.62 (m, 2H); 1.60−1.48 (m, 4H); 1.42−1.14 (m, 20H); 1.13 (s, 9H).

ESI-TOF HRMS m/z calcd. for $C_{72}H_{95}N_{10}O_{14}S2^+$ $[M+H^+]$ 1387.6465, found 1386.9774.

2.3.2. Synthesis of Thiosaccharides. The detailed synthetic procedure is reported only for the final product 1-mercapto-2,3,4,6-tetra-*O*-acetyl-D-glucopyranose (**14G**). Compounds **14L** and **14M** were obtained through the same pathways using an α- and β-mixture of D-lactose and maltotriose, respectively, as starting materials instead of D-(+)-glucose.

*Synthesis of Acetylated Sugars (**10G**, **10L**, **10M**).* A suspension of sodium acetate (1.6 g, 19.3 mmol) in acetic anhydride (22.5 g, 220.5 mmol) was refluxed for 30 min. Then, glucose (9G; 3.2 g, 17.5 mmol) was added, and the reaction mixture was refluxed for an additional 3.5 h (TLC: CH/EtOAc 4:6) and then slowly poured into ice while still hot. The formation of a precipitate was observed that was collected by filtration and washed with water to yield **1,2,3,4,6-penta-*O*-acetyl-D-glucopyranose** (**10G**; 5.6 g, 14.3 mmol, 82% yield).

^{1}H NMR (400 MHz, $CDCl_3$): δ 5.73−5.69 (d, J = 8.2 Hz, 1H); 5.28−5.22 (t, J = 9.4 Hz, 1H); 5.16−5.09 (m, 2H); 4.31−4.26 (dd, J = 12.1 Hz, 4.5 Hz, 1H); 4.13−4.08 (dd, J = 12.5 Hz, 2.1 Hz, 1H); 3.86−3.81 (m, 1H); 2.11 (s, 3H); 2.08 (s, 3H); 2.03 (s, 6H); 2.00 (s, 3H).

1,2,3,6-Tetra-*O*-acetyl-4-*O*-(2,3,4,6-tetra-*O*-acetyl-α-D-galactopyranosyl)-α-D-galactopyranose (10L)

1.1 g, 1.6 mmol, 86% yield. **^{1}H NMR** (400 MHz, $CDCl_3$): δ 5.68−5.65 (d, J = 8.2 Hz, 1H); 5.36−5.43 (m, 1H); 5.27−5.21 (t, J = 9.3 Hz, 1H); 5.13−5.02 (m, 2H); 4.97−4.93 (dd, J = 3.4 Hz, 10.6 Hz, 1H); 4.49−4.43 (m, 2H); 4.16−4.05 (m, 3H); 3.89−3.83 (m, 2H); 3.78.3.73 (m, 1H); 2.15 (s, 3H); 2.12 (s, 3H); 2.09 (s, 3H); 2.07 (s, 3H); 2.05 (s, 3H); 2.04 (s, 3H); 2.03 (s, 3H); 1.96 (s, 3H).

1,2,3,6-Tetra-*O*-acetyl-4-*O*-(2,3,6-tri-*O*-acetyl-4-*O*-(2,3,4,6-tetra-*O*-acetyl-α-*O*-glucopyranosyl)-α-D glucopyranosyl)-α-D-glucopyranose (10M)

1.7 g, 1.8 mmol, 90% yield. **^{1}H NMR** (400 MHz, DMSO-d_6): δ 5.93−5.89 (d, J = 8.1 Hz, 1H); 5.50−5.45 (t, J = 8.8 Hz, 1H); 5.29−5.17 (m, 4H); 5.10−4.95 (t, J = 9.9 Hz, 1H); 4.88−4.75 (m, 3H); 4.37−4.28 (m, 2H); 4.24−4.13 (m, 4H); 4.03−3.93 (m, 5H); 2.08−2.06 (m, 6H); 2.05 (s, 3H); 2.01 (s, 3H); 1.98 (s, 6H); 1.97−1.94 (m, 15H).

Bromination of Acetylated Sugars. To a solution of **10G** (1.0 g, 2.6 mmol) in CH_2Cl_2 (6.5 mL), 30% HBr in CH_3COOH (7.8 mL) was added. The reaction mixture was stirred at room temperature for 30 min (TLC: CH/EtOAc 4:6). The reaction mixture was added dropwise to a saturated $NaHCO_3$ solution previously cooled to 0 °C and then extracted with CH_2Cl_2. The organic layer was dried over anhydrous Na_2SO_4, filtered, and concentrated under vacuum to yield **1-bromo-2,3,4,6-tetra-*O*-acetyl-D-glucopyranose** (**11G**; 0.8 g, 1.95 mmol, 75% yield).

https://doi.org/10.1021/acs.molpharmaceut.4c00124
Mol. Pharmaceutics 2024, 21, 3848−3865

^{1}H NMR (400 MHz, $CDCl_3$): δ 6.62−6−60 (d, J = 4.2 Hz, 1H); 5.59−5.53 (t, J = 9.9 Hz, 1H); 5.19−5.13 (t, J = 9.7 Hz, 1H); 4.86−4.82 (dd, J = 4.0 Hz, 10.3 Hz, 1H); 4.35−4.27 (m, 2H); 4.15−4.12 (d, J = 10.6 Hz, 1H); 2.10 (s, 3H); 2.09 (s, 3H); 2.05 (s, 3H); 2.03 (s, 3H).

1-Bromo-2,3,6-tri-*O*-acetyl-4-*O*-(2,3,4,6-tetra-*O*-acetyl-*α*-D-galactopyranosyl)-*α*-D-galactopyranose (11L)

1.2 g, 1.7 mmol, quantitative yield. **^{1}H NMR** (400 MHz, $CDCl_3$): δ 6.54−6.51 (d, J = 4.2 Hz, 1H); 5.59−5.52 (t, J = 9.4 Hz, 1H); 5.37−5.53 (d, J = 2.9 Hz, 1H); 5.15−5.10 (dd, J = 7.4 Hz, 10.3 Hz, 1H); 4.98−4.94 (dd, J = 3.4 Hz, 10.5 Hz, 1H); 4.78−4.74 (dd, J = 4.6 Hz, 10.3 Hz, 1H); 4.53−4.47 (m, 2H); 4.23−4.05 (m, 4H); 3.91−3.83 (m, 2H); 2.16 (s, 3H); 2.13 (s, 3H); 2.09 (s, 3H); 2.07 (s, 3H); 2.06 (s, 3H); 2.05 (s, 3H); 1.97 (s, 3H).

1-Bromo-2,3,6-Tri-*O*-acetyl-4-*O*-(2,3,6-tri-*O*-acetyl-4-*O*-(2,3,4,6-tetra-*O*-acetyl-*α*-*O*-glucopyranosyl)-*α*-D-glucopyranosyl)-*α*-D-**glucopyranose (11M)**

1.7 g, 1.6 mmol, 90% yield. **^{1}H NMR** (400 MHz, DMSO-d_6): δ 5.44−5.38 (t, J = 9.2 Hz, 1H); 5.30−5.17 (m, 4H); 5.02−4.95 (t, J = 9.9 Hz, 1H); 4.91−4.83 (td, J = 10.6 Hz, 3.7 Hz, 2H); 4.82−4.77 (dd, J = 10.6 Hz, 3.7 Hz, 1H); 4.43−4.12 (m, 8H); 4.05−3.93 (m, 4H); 2.08 (s, 3H); 2.07 (s, 3H); 2.03−1.94 (m, 27H).

Synthesis of Acetylated Glycosilthiuronium Hydrobromides. **11G** (0.8 g, 1.9 mmol) was dissolved in acetone (4 mL), and then, thiourea (0.2 mg, 2.9 mmol) was added. The reaction mixture was refluxed for 3 h (TLC: CH/EtOAc 4:6). At completion of the reaction, the mixture was cooled to room temperature and concentrated under reduced pressure to yield **2,3,4,6-tetra-*O*-acetyl-D-glucopyranosylthiuronium hydrobromide (12G**; 0.9 g, 1.9 mmol, quantitative yield).

^{1}H NMR (400 MHz, DMSO-d_6): δ 9.24 (s, 2H); 9.06 (s, 2H); 5.70−5.65 (d, J = 10.2 Hz, 1H); 5.35−5.29 (t, J = 9.4 Hz, 1H); 5.15−5.08 (m, 2H); 4.23−4.15 (m, 2H); 4.11−4.06 (m, 1H); 2.06 (s, 3H); 2.02 (s, 3H); 2.00 (s, 3H); 1.98 (s, 3H).

2,3,6-Tri-*O*-acetyl-4-*O*-(2,3,4,6-tetra-*O*-acetyl-*α*-D-galactopyranosyl)-*α*-D-galactopyranosylthiuronium hydrobromide (12L)

1.14 g, 1.5 mmol, quantitative yield. **^{1}H NMR** (400 MHz, D_2O): δ 5.48−5.43 (m, 2H); 5.36−5.31 (m, 1H); 5.29−5.25 (d, J = 9.4 Hz, 1H); 5.24−5.18 (m, 1H); 5.06−5.00 (t, J = 8.4 Hz, 1H); 4.85−4.83 (d, J = 7.8 Hz, 1H); 4.60−4.55 (d, J = 12.1 Hz, 1H); 4.28−4.20 (m, 5H); 4.11−4.05 (m, 1H); 2.22 (s, 3H); 2.18 (s, 3H); 2.16 (s, 3H); 2.15 (s, 3H); 2.13 (s, 6H); 2.02 (s, 3H).

2,3,6-Tri-*O*-acetyl-4-*O*-(2,3,6-tri-*O*-acetyl-4-*O*-(2,3,4,6-tetra-*O*-acetyl-*α*-*O*-glucopyranosyl)-*α*-D-glucopyranosyl)-*α*-D-**glucopyranosylthiuronium hydrobromide (12M)**

1.7 g, 1.6 mmol, quantitative yield. **^{1}H NMR** (400 MHz, DMSO-d_6): δ 9.26 (s, 2H); 9.03 (s, 2H); 5.68−5.64 (d, J = 10.2 Hz, 1H); 5.39−5.35 (t, J = 8.8 Hz, 1H); 5.28−5.25 (m, 2H); 5.21−5.17 (m, 2H); 5.01−4.95 (t, J = 9.3 Hz, 2H); 4.88−4.83 (m, 1H); 4.80−4.74 (m, 1H); 4.20−4.10 (m, 5H); 4.04−3.92 (m, 6H); 2.09−2.07 (m, 6H); 2.02 (s, 3H); 2.01 (s, 3H); 1.99−1.97 (m, 9H); 1.97−1.94 (m, 9H).

Synthesis of Acetylated Glycosyl Thiols. **12G** (0.9 g, 1.8 mmol) and $Na_2S_2O_5$ (0.5 g, 2.5 mmol) were added to a 1:1 mixture of CH_2Cl_2:H_2O (9 mL). The reaction mixture was heated to 70 °C for 3.5 h (TLC: $CHCl_3$/MeOH 9:1); then, it was cooled down to room temperature, diluted with CH_2Cl_2, and washed with a saturated NH_4Cl solution. The organic layer was dried with anhydrous Na_2SO_4, then filtered, and concentrated under vacuum to yield the crude product, which was purified by column chromatography ($CHCl_3$/MeOH 95:5) to yield **1-mercapto-2,3,4,6-tetra-*O*-acetyl-D-glucopyranose (13G**; 0.3 g, 0.81 mmol, 45% yield).

H NMR (400 MHz, $CDCl_3$): δ 5.18−5.13 (t, J = 9.4 Hz, 1H); 5.09−5.03 (t, J = 9.8 Hz, 1H); 4.96−4.90 (t, J = 9.5 Hz, 1H); 4.55−4.49 (t, J = 9.9 Hz, 1H); 4.23−4.18 (dd, J = 12.5 Hz, 4.9 Hz, 1H); 4.1−4.1 (dd, J = 12.5 Hz, 2.4 Hz, 1H); 3.72−3.67 (m, 1H); 2.31−2.28 (d, J = 10.0 Hz, 1H); 2.05 (s, 3H); 2.04 (s, 3H); 1.98 (s, 3H); 1.96 (s, 3H).

1-Mercapto-2,3,6-tri-*O*-acetyl-4-*O*-(2,3,4,6-tetra-*O*-acetyl-*α*-D-galactopyranosyl)-*α*-D-galactopyranose (13L)

It was obtained using the same synthetic pathway above. 0.18 g, 0.3 mmol, 93% yield. **^{1}H NMR** (400 MHz, $CDCl_3$): δ 5.19−5.14 (t, J = 9.2 Hz, 1H); 5.11−5.05 (m, 1H); 4.95−4.91 (dd, J = 11.0 Hz, 3.4 Hz, 1H); 4.89−4.84 (t, J = 9.5 Hz, 1H); 4.55−4.41 (m, 3H); 4.14−4.04 (m, 4H); 3.88−3.83 (m, 1H); 3.81−3.76 (t, J = 9.7 Hz, 1H); 3.64−3.59 (m, 1H); 2.14 (s, 3H); 2.12 (s, 3H); 2.08 (s, 3H); 2.05 (s, 3H); 2.03 (s, 3H); 2.02 (s, 3H). 1.95 (s, 3H).

1-Mercapto-2,3,6-Tri-*O*-acetyl-4-*O*-(2,3,6-tri-*O*-acetyl-4-*O*-(2,3,4,6-tetra-*O*-acetyl-*α*-*O*-glucopyranosyl)-*α*-D-glucopyranosyl)-*α*-D-**glucopyranose (13M)**

It was obtained using the same synthetic pathway above. 0.26 g, 0.3 mmol, 83% yield. **^{1}H NMR** (400 MHz, $CDCl_3$): δ 5.45−5.23 (m, 6H); 5.11−5.04 (t, J = 9.4 Hz, 1H); 4.89−4.83 (m, 1H); 4.81−4.72 (m, 2H); 4.53−4.43 (m, 2H); 4.35−3.90 (m, 10H); 2.15 (s, 3H); 2.10 (s, 6H); 2.06−1.99 (m, 21H).

Synthesis of Glycosyl Thiols. A solution of **13G** (0.3 g, 0.8 mmol) in MeOH (2 mL) was added to 1 mL of 0.55 M methanolic sodium methoxide (27.4 mg, 0.55 mmol). The reaction mixture was stirred at room temperature for 16 h (TLC: $CHCl_3$/MeOH 9:1). The crude mixture was quenched by the addition of DOWEX (50WX8 hydrogen form 100−200 mesh). After filtration, the solution was concentrated to yield **1-mercapto-D-glucopyranose (14G**; 0.2 g, 0.8 mmol, quantitative yield).

^{1}H NMR (400 MHz, D_2O): δ 4.58−4.55 (d, J = 9.5 Hz, 1H); 3.91−3.87 (dd, J = 12.6 Hz, 2.1 Hz, 1H); 3.37−3.68 (dd, J = 12.1 Hz, 5.5 Hz, 1H); 3.51−3.42 (m, 3H); 3.30−3.25 (t, J = 9.3 Hz, 1H).

1-Mercapto-4-*O*-(*β*-D-galactopyranosyl)-D-glucopyranose [Thiolactose] (14L)

0.1 g, 0.3 mmol, quantitative yield. **^{1}H NMR** (400 MHz, D_2O): 4.60−4.57 (d, J = 9.6 Hz, 1H), 4.47−4.44 (d, J = 7.5 Hz, 1H), 4.00−3.50 (m, 12H).

1-Mercapto-4-*O*-[4-*O*-(*α*-D-glucopyranosyl)*α*-D-glucopyranosyl]-D-glucopyranose [Thiomaltotriose] (14M)

0.1 g, 0.1 mmol, quantitative yield, **^{1}H NMR** (400 MHz, D_2O): 5.42−5.38 (m, 2H), 4.60−4.55 (d, J = 9.7 Hz, 1H), 4.00−3.56 (m, 16H), 3.45−3.40 (t, J = 9.7 Hz, 1H), 3.34−3.27 (t, J = 9.2 Hz, 1H).

2.3.3. Synthesis of IP-002$_x$-Rho. The detailed synthetic procedure is reported below for IP-002$_G$-Rho (**15**). Compounds **16** and **17** were obtained with analogue methods, starting from the appropriate thiosugars.

To a solution of **IP-002-Rho** (10.0 mg, 7.2 μmol) in EtOH (2 mL), 14 M (19.6 mg, 0.1 mmol), propionitrile (2 mL), and TEA (20 μL) were added. The reaction mixture was stirred under a N_2 atmosphere at room temperature for 24 h (TLC: $CHCl_3$/MeOH 9:1). The reaction mixture was diluted with 10 mL of an EtOAc/EtOH 6:4 mixture and washed with a saturated NH_4Cl solution (2 mL × 10 mL). The organic layer

https://doi.org/10.1021/acs.molpharmaceut.4c00124
Mol. Pharmaceutics 2024, 21, 3848−3865

was dried over anhydrous Na_2SO_4, filtered, and concentrated under vacuum to yield the crude product, which was purified by preparative HPLC to yield **IP-002$_G$-Rho** (1.7 mg, 1.1 μmol, 15% yield).

^{1}H NMR (400 MHz, CD_3OD): δ 8.73 (d, *J* = 1.7 Hz, 1H); 8.15−8.11 (dd, *J* = 7.8 Hz, 1.4 Hz, 1H); 7.61−7.57 (m, 1H); 7.52−7.47 (m, 2H); 7.40−7.36 (d, *J* = 7.8 Hz, 1H); 7.32−7.23 (m, 3H); 7.14−7.09 (m, 3H); 7.08−7.03 (m, 1H); 7.00−6.92 (m, 2H); 6.82−6.79 (m, 1H); 6.74−6.79 (m, 1H); 5.20−5.15 (d, *J* = 18.1 Hz, 1H); 4.55−4.50 (m, 1H); 4.38−4.32 (d, *J* = 18.3 Hz, 1H); 3.94−3.86 (m, 2H); 3.70−3.54 (m, 21H); 3.30−3.10 (m, 11H); 2.85−2.60 (m, 3H); 2.10−2.02 (m, 1H); 1.88−1.80 (m, 1H); 1.79−1.72 (m, 1H); 1.70−1.24 (m, 27H); 1.22 (s, 9H).

HRMS *m*/*z* calcd. for $C_{78}H_{107}N_{10}O_{19}S_3^+$ [M + H$^+$] 1583.6871, found 1582.7345.

IP-002$_L$-Rho (16). [IP-002-Rho]:[Thiolactose] = 1:12.35, reaction time: 48 h, and reaction T: 45 °C.

Yield: 2.6 mg. 1.5 μmol, 19%.

^{1}H NMR (400 MHz, CD_3OD): δ 8.72 (d, *J* = 1.5 Hz, 1H); 8.15−8.11 (dd, *J* = 7.9 J = 1.5 Hz, 1H); 7.60−7.55 (m, 1H); 7.53−7.48 (m, 2H); 7.39−7.35 (d, *J* = 7.7 Hz, 1H); 7.31−7.23 (m, 3H); 7.14−7.08 (m, 3H); 7.06−7.03 (d, *J* = 7.6 Hz, 1H); 7.00−6.92 (m, 2H); 6.83−6.80 (m, 1H); 6.75−6.70 (m, 1H); 5.20−5.15 (d, *J* = 17.9 Hz, 1H); 4.55−4.50 (m, 1H); 4.40−4.33 (d, *J* = 15.9 Hz, 1H); 4.02−3.10 (m, 41H); 2.85−2.54 (m, 3H); 2.10−2.03 (m, 1H); 1.88−1.81 (m, 1H); 1.79−1.72 (m, 1H); 1.70−1.24 (m, 27H); 1.22 (s, 9H).

HRMS *m*/*z* calcd. for $C_{84}H_{117}N_{10}O_{24}S_3^+$ [M + H$^+$] 1745.7399, found 1745.7410.

IP-002$_M$-Rho (17). [IP-002-Rho]:[Thiomaltotriose] = 1:35.1; reaction time: 48 h, reaction temperature: 45 °C, and 1.5 mL of DI water instead of 2 mL of proprionitrile.

Yield: 3.3 mg, 1.7 μmol, 30%.

^{1}H NMR (400 MHz, CD_3OD): δ 8.73 (d, *J* = 1.5 Hz, 1H); 8.16−8.11 (dd, *J* = 7.9, 1.5 Hz, 1H); 7.62−7.56 (m, 1H); 7.57−7.46 (m, 2H); 7.40−7.36 (d, *J* = 7.7 Hz, 1H); 7.33−7.23 (m, 3H); 7.14−7.09 (m, 3H); 7.08−7.05 (d, *J* = 7.9 Hz, 1H); 7.00−6.93 (m, 2H); 6.83−6.80 (m, 1H); 6.74−6.70 (m, 1H); 5.20−5.25 (d, *J* = 15.9 Hz, 1H); 4.56−4.50 (m, 1H); 4.41−4.35 (d, *J* = 15.9 Hz, 1H); 4.00−3.10 (m, 48H); 2.83−2.54 (m, 3H); 2.10−2.02 (m, 1H); 1.88−1.82 (m, 1H); 1.80−1.74 (m, 1H); 1.70−1.24 (m, 27H); 1.22 (s, 9H).

HRMS *m*/*z* calcd. for $C_{90}H_{127}N_{10}O_{29}S_3^+$ [M + H$^+$] 1907.7927, found 1907.6882.

2.3.4. Synthesis of IP-002$_H$-Rho. To a solution of **8** (6.3 mg, 6.8 μmol) in EtOH (1 mL) 10% (catalytic) Pd/C was added. The reaction mixture was saturated with gaseous hydrogen and stirred for 18 h at room temperature (TLC: $CHCl_3$/MeOH 9:1). The reaction mixture was filtered to remove the catalyst and dried under reduced pressure to yield **IP-002$_H$-Rho** (5.7 mg, 6.2 μmol, 91% yield).

^{1}H NMR (400 MHz, CD_3OD): δ 8.30−8.20 (m, 1H); 8.13−8.05 (m, 1H); 7.94−7.83 (m, 1H); 7.76−7.68 (m, 1H); 7.45−7.42 (m, 2H); 7.40−7.15 (m, 6H); 7.13−7.02 (m, 2H); 7.02−6.93 (m, 1H); 6.82−6.75 (d, J = 14.3, 1H); 6.23−6.15 (m, 1H); 5.20−5.13 (d, *J* = 17.9, 1H); 4.60−4.46 (m, 1H); 4.38−4.32 (d, *J* = 17.9, 1H); 3,76−3.32 (m, 18H); 3.28−3.08 (m, 15H); 2.68−2.65 (m, 3H); 2.44−2.41 (m, 3H); 2.10−1.20 (m, 31H).

ESI-TOF HRMS *m*/*z* calcd. for $C_{72}H_{97}N_{10}O_{14}S$ [M+H$^+$] 1389.6622, found 1389.6635.

2.4. Molecular Docking. Nastorazepide and **IP-002$_G$-Rho** were docked into CCK2-R (PDB-ID: 7f8w) through SeeSAR ver. 12.1.0 software [SeeSAR version 12.1.0; BioSolveIT GmbH, Sankt Augustin, Germany, 2021, www.biosolveit.de/SeeSAR]. Ligand tridimensional structures and protonation states were obtained using the internal tool of SeeSAR starting from the SMILES code. For each ligand, the single top-scoring pose was analyzed.

2.5. IP-002$_x$-Rho Solubility Studies. Solubility tests were performed by diluting 5 μL of IP-002$_x$-Rho stock solutions in DMSO (5 mg/mL) in 150 μL of PBS. The saturated solutions were then centrifuged at 12,000 rpm for 5 min and analyzed by RP-HPLC. The quantification was performed based on a calibration curve obtained with sulforhodamine B in the 0.1−1 μM concentrations range in PBS ($y = 2 \times 10^6 x + 1896.7$, R^2 = 0.9998).

2.6. Synthesis of Gelatin Methacrylate (GelMA). GelMA was prepared according to the protocol reported by the group of Demirci,[33] with slight modifications.

Briefly, a 10% w/V gelatin (from porcine skin, powder gel strength 300 g Bloom; type A, by Sigma-Aldrich) solution was prepared in PBS preheated at 50 °C. The solution was left under stirring for 1 h, and then, 8 mL of methacrylic anhydride (8.28 g, 53.7 mmol) was added dropwise. The reaction solution was left under stirring at 50 °C for 2.5 h and then transferred into a 3.5 kDa MWCO dialysis bag and dialyzed against DI water at 40−45 °C for 7 to 15 days until complete removal of unreacted species. The solution was then freeze-dried, and lyophilized GelMA was stored at −20 °C until use.

2.7. GelMA Scaffold Fabrication and Rheological Characterization. GelMA (16, 20, 25% w/V) was suspended in PBS or DMEM-F12 and heated to 70−75 °C in a water bath. At complete solubilization, 0.5% w/V lithium phenyl-2,4,6-trimethylbenzoylphosphinate (LAP) was added, and the solution was kept in the dark. The solution was sterilized by a STERISTEAM 2 autoclave (121 °C for 15 min) and then cooled to room temperature. The solution was then cast on an in-house built 6-well mold, and 8 mm × 5 mm scaffolds were generated by cross-linking GelMA by 3 min near UV irradiation (λ = 365 nm, 230 W·m^{-2} average light intensity). The viscoelastic properties of the hydrogels were evaluated using a Discovery HR-2 Hybrid rheometer (TA Instruments, New Castle, Delaware) equipped with a parallel plate geometry (40 mm) and a Peltier system for temperature control.

A temperature sweep measurement was performed to evaluate the storage (G') and loss (G'') moduli as a function of temperature. The hydrogels were tested from 15 to 50 °C, with a temperature ramp of 2 °C/min, at a fixed frequency of 1 Hz and a shear strain of 0.05. Three specimens (diameter: 35 mm, thickness: 2 mm) for each GelMA concentration (10, 16, 20, and 25%) were tested.

2.8. In Vitro Studies. *2.8.1. Cell Culture.* A431 WT (cell type of human epidermoid carcinoma) was purchased from the American Type Culture Collection (ATCC) cell bank (Manassas, VA). The A431-CCK2-R$^+$ cell line was kindly provided by Prof. Rosalba Mansi.[34] A431 WT and A431-CCK2-R$^+$ cells were cultured in the monolayer in Dulbecco's modified Eagle medium (DMEM high glucose) supplemented with 10% (v/v) FBS, 2.0 mM L-glutamine, 100.0 IU/mL penicillin, and 100.0 μg/mL streptomycin. A concentration of 0.5 mg/mL Geneticin was maintained for the cultivation of A431-CCK2-R$^+$. Cells were incubated in a humidified atmosphere with 5% CO_2 at 37 °C.

https://doi.org/10.1021/acs.molpharmaceut.4c00124
Mol. Pharmaceutics 2024, 21, 3848−3865

2.8.2. Cell Line Characterization. Western Blot. A431 WT or A431-CCK2-R$^+$ cells were lysed in situ with 500 μL of RIPA lysis buffer supplemented with protease inhibitors (RIPA lysis buffer system, sc-24948, Santa Cruz Biotechnologies) at 4 °C for 30 min. Lysates were clarified by centrifugation at 12,000× g at 4 °C for 15 min. Proteins were quantified with the DC protein assay (Bio-Rad). 40 μg of proteins in each sample was separated using Bolt Bis-Tris Plus precast 8% polyacrylamide gels and MOPS SDS running buffer (Thermo Fisher). Afterward, proteins were blotted onto PVDF membranes. After blocking with TBS containing 0.1% Tween 20 and 5% BSA (blocking buffer) for 2 h at room temperature, membranes were incubated overnight at 4 °C with antihuman CCK2-R mouse monoclonal antibodies conjugated with phycoerythrin (clone E-3, sc-166690, Santa Cruz Biotechnology) diluted at 1:400 in blocking buffer. Fluorescent signals were detected with a ChemiDoc instrument (Bio-Rad) using the Cy3 filter. To normalize over the protein load, membranes were subsequently incubated overnight at 4 °C with rabbit antihuman GAPDH antibodies (Santa Cruz Biotechnologies) diluted at 1:500 in blocking buffer. Signals were detected by 1 h incubation at room temperature with HRP-conjugated secondary antibodies (Abcam, AB6013), followed by incubation with an ECL detection reagent (Thermo Fisher) and ChemiDoc imaging (Bio-Rad).[27]

Calcium Imaging with Fura-2/AM. A431 WT or A431-CCK2-R$^+$ (5×10^5 cells/well) was seeded on 18 mm coverslips and grown in DMEM + 10% (V/V) FBS, with the addition of a 0.5 μg/mL Geneticin solution for A431-CCK2-R$^+$, and grown for 24 h. Cells were then incubated with 1 μM Fura-2/AM, 0.02% w/V pluronic F-127, and 200 μM sulfinpyrazone in 1 mL of mKRB medium (140 mM NaCI, 2.8 mM KCI, 2 mM $MgCl_2$, 10 mM HEPES, 1 mM $CaCl_2$, 10 mM glucose, pH 7.4) for 40 min at 37 °C. After 3× washing with 1 mL of mKRB, coverslips were mounted in a chamber, and fresh mKRB was added. Fura-2-loaded cells were visualized by a 40× ultraviolet-permeable objective (Olympus Biosystems GmbH, Planegg, Germany) on an inverted microscope (Zeiss Axiovert 100, Jena, Germany). Alternating excitation wavelengths of 340 and 380 nm were obtained by a monochromator (polychrome V, TILL-Photonics) controlled by custom-made software (Roboscope, developed by Catalin Dacian Ciubotaru at VIMM, Padua, Italy). A neutral density filter, UVND 0.6 (Chroma), was used in the excitation pathway. The emitted fluorescence was collected at 500−530 nm. Biological activity was measured by stimulating the cells with a 10 μM CCK-8 or gastrin I solution in DMSO with or without 2 min of preincubation with a 1 μM Z-360 solution and monitoring fluorescence over 400 s. Images were acquired every second, with 200 ms exposure time at each wavelength, by a PCO SensiCam QE (Kelheim, Germany) camera controlled by the same Roboscope software. Regions of interest corresponding to the cytoplasmic regions were selected for the calculation of the ratio (R) between the two fluorescence intensities (340 and 380 nm), which is proportional to $[Ca^{2+}]$. To calculate the percentage of cells displaying Ca^{2+} oscillations, a threshold corresponding to the basal 340/380 nm R + 1 SD of A431-CCK2-R$^+$ or A431 WT cells was set. The cells displaying R values above the threshold upon stimulation with gastrin I were considered to be positive. Data were plotted with GraphPad Prism software v9.2.

Uptake and Competition Test with CCK-8(FAM). Cellular uptake of CCK-8 (FAM) was assessed on both cell lines. A431 WT or A431-CCK2-R$^+$ (1.5×10^5 cells/well) was seeded on 24-well plates and grown for 24 h. For uptake studies, cells were incubated with 400 μL of 5 μg/mL CCK-8 (FAM) solution in complete medium for 30 min at 37 °C. For competition studies, cells were pretreated with 400 μL of 50 μg/mL gastrin I solution for 30 min followed by the addition of 2 μL of 1 mg/mL CCK-8 (FAM) stock solution in DMSO. Untreated cells were used as the control. Then, cells were washed 3 mL × 0.5 mL with PBS, detached with 200 μL of 0.5 × trypsin-EDTA solution, and fixed with 200 μL of 1% paraformaldehyde (PFA) in FACS buffer (0.1% BSA, 2 mM EDTA, 2 mM NaN_3 in PBS) before flow cytometry (FC) analysis. Flow cytometric measurements were performed on an FC500 instrument (Beckman Coulter). A 488 nm laser was used for excitation and scattering, and emission was detected in channel FL-1 with a 527 BP filter. At least 10^4 events were recorded per sample and data were processed with FlowJo software v10.0. Three independent experiments with three biological replicates were performed.

2.8.3. IP-002$_x$-Rho 2D Cell Association and Competition Studies. The A431 WT and A431-CCK2-R$^+$ (1.5×10^5 cells/well) were seeded on 24-well plates and cultivated for 24 h.

Association Study. Cells were incubated with 400 μL of 0.5 μg/mL solutions of each molecule (obtained by diluting in complete medium 2 μL of IP-002$_x$-Rho stock solution in DMSO) for 30 min. Untreated cells added of 2 μL of pure DMSO in the culture medium were used as the control.

Competition Tests. For competition studies, cells were preincubated with 400 μL of 50 μg/mL gastrin I solution in complete medium for 30 min before the addition of 2 μL of 100 μg/mL IP-002$_x$-Rho stock solutions in DMSO. Cells were then further incubated for 30 min. Untreated cells added of 2 μL of pure DMSO after the first 30 min of incubation were used as a control. A second competition study was carried out by preincubating cells with medium only or 0.136 μg/mL (262 nM) Z-360 solution in complete medium for 30 min followed by addition of equimolar concentration of IP-002$_H$-Rho and IP-002$_M$-Rho. Samples were then treated as described above.

After the incubation time, the medium was discarded and the cells were washed three times with 0.5 mL of PBS, detached with 200 μL of 0.5 × trypsin-EDTA solution, and diluted with 200 μL of 1% PFA in FACS buffer before FC analysis. Samples were analyzed on a BD FACSAria III cell sorter running the BD FACSDiva software. A 488 nm laser was used for excitation and scattering, and emission was detected in the PE channel. At least 10^4 events were recorded per sample, and data were analyzed with FlowJo software v10.0. Three independent experiments were performed in triplicate.

2.8.4. IP-002$_M$-Rho Trafficking Study and Colocalization Analysis. IP-002$_M$-Rho internalization pathways were evaluated by confocal microscopy studies.

A431-CCK2-R$^+$ cells were seeded on 12 mm coverslips in a 24-well plate (1.0×10^5 cells/well) 24 h before the experiment. Cells were incubated with 2 or 4 μg/mL IP-002$_M$-Rho in complete medium (400 μL) at 37 °C for 30 min or 1 h, then washed with PBS (3 μL × 500 μL), fixed in 4% PFA in PBS (200 μL) at room temperature for 10 min, and rinsed with PBS (3 μL × 500 μL). Only in samples with endosomal staining, cells were then permeabilized in 0.5% Tween 20 in PBS (200 μL) for 10 min at room temperature, rinsed with PBS (3 μL × 500 μL), and incubated with 200 μL of blocking solution (4% Bovine Serum Albumine in PBS) for 1 h at room temperature. After washing with PBS (3 μL × 500 μL), cells were incubated

https://doi.org/10.1021/acs.molpharmaceut.4c00124
Mol. Pharmaceutics 2024, 21, 3848−3865

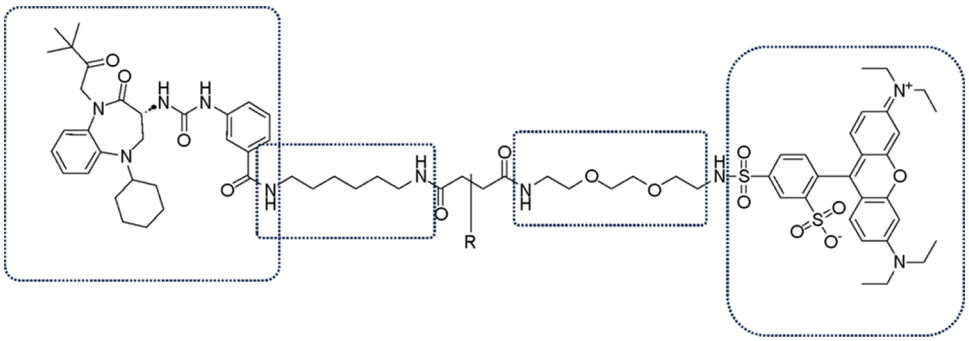

Figure 1. General structures of the synthesized final fluorescent ligands **IP-002$_G$-Rho** (R = thioglucose), **IP-002$_L$-Rho** (R = thiolactose), **IP-002$_M$-Rho** (R = thiomaltotriose), and **IP-002$_H$-Rho** (R = H). Each moiety was highlighted to facilitate an understanding of the synthetic procedure.

with the rabbit anti-human EEA1 primary antibody (200 μL, 1:100 dilution in blocking buffer) for 1 h at room temperature, rinsed again 3 mL × 0.5 mL with PBS, and incubated with the Alexa Fluor™ 488-conjugated goat anti-rabbit secondary antibody (200 μL, 1:300 dilution in blocking buffer) for further 1 h at room temperature. For all samples, cell nuclei were stained with 2 μM Hoechst 33258 in PBS (200 μL) at room temperature for 15 min. Finally, coverslips were washed three times with 0.5 mL of PBS and mounted onto microscope slides with ProLong Glass Antifade mounting solution. The slides were left at 4 °C overnight before confocal microscopy analysis.

The microscope slides were observed under a Zeiss LSM 800 confocal laser-scanning microscope (Carl Zeiss Microscopy, Oberkochen, Germany) equipped with a 40× (air) or 63× (immersion) objective. Hoechst 33258, Alexa Fluor 488, and sulforhodamine were excited with a 405, 488, and 561 nm laser, respectively. Images were acquired as *z*-stacks with increments of 800 nm and processed with Zen 3.9 software Blue edition (Zeiss, Germany).

The colocalization of IP-002$_M$-Rho with anti-EEA1-labeled endosomes was evaluated by Pearson's coefficient (PC) in ROIs taken from acquired images using the Coloc 2 Fiji plugin. Standard deviation was calculated as variation between mean PC values.

2.8.5. GelMA Scaffold Fabrication with Embedded Cells. 16% (w/V) GelMa solution was prepared as described in paragraph 2.7 "GelMA Scaffold Fabrication and Rheological Characterization". After GelMA solution sterilization, 3.0×10^5 A431 WT or A431-CCK2-R$^+$ cells were suspended in 200 μL volume of sterile GelMA solution. The suspension was then cast on an in-house built 6-well mold and 8 mm × 5 mm scaffolds were generated cross-linking GelMA by 3 min near-UV irradiation (λ = 365 nm, 230 W·m^{-2} average light intensity). Scaffolds with embedded cells were then transferred to a 24-well plate and incubated in DMEM complete medium (added of 0.5 mg/mL Geneticin for A431-CCK2-R$^+$ seeded scaffolds) for 3 days before use.

2.8.6. Cellularized GelMA Scaffold Characterization: Cell Morphology and Vitality. A431 WT and A431-CCK2-R$^+$-cellularized scaffolds were prepared as described in paragraph 2.8.5 "GelMa Scaffold Fabrication with Embedded Cells" and used at day 4 postfabrication. Scaffolds were washed twice with 400 μL of PBS and treated as follows.

Cell Viability. A live−dead assay was performed to assess the viability of cells embedded in the scaffolds. Live/dead cells were stained by incubating cellularized scaffolds with 1 mL of 1 μg/mL Calcein AM and 20 μg/mL Propidium Iodide (PI) in PBS used at 37 °C for 10 min. Live cell (green) and dead cell (red) percentages were calculated from the ratio of the green or red area on the total color area in the *z*-axis projection of the 3D image.

Cell Morphology. Cells embedded in the scaffolds were stained with DAPI and Oregon Green 488 phalloidin to assess the cell morphology. Cells embedded in scaffolds were fixed in 4% PFA in PBS (500 μL) at room temperature for 45 min. Afterward, samples were washed twice with 500 μL of PBS. Cells were then permeabilized in 500 μL of 0.1% Triton X-100 in PBS at room temperature for 45 min, washed twice with 500 μL of PBS, and incubated at room temperature for 45 min with 500 μL of staining solution prepared diluting 5.6 μL of DAPI stock solution (Sigma-Aldrich) in 25 mL of PBS and adding 1 μL of Oregon Green 488 phalloidin stock solution (Thermo Fisher Scientific).

Cellularized scaffolds were observed using a Nikon ECLIPSE Ti inverted fluorescence microscope for super-resolution imaging, collecting multistack pictures by laser excitation at 488 nm (Calcein, Oregon Green), 405 nm (DAPI), or 561 nm (PI) and collecting fluorescence emission through 525/50 nm (Calcein, Oregon Green), 450/50 nm (DAPI), and 595/50 (PI) band-pass filters.

2.8.7. Association Studies in GelMA-Cellularized Scaffolds. Scaffolds were produced as previously described, seeded with A431 WT or A431-CCK2-R$^+$ cells, and kept at 37 °C in a humidified incubator for 4 days prior to the treatment. Cell association of the developed compounds was assessed by incubating the scaffolds with 400 μL of 25 μg/mL IP-002$_x$-Rho solution in complete medium (DMEM + 10% FBS) for 4 or 18 h. After treatment, the scaffolds were washed three times with 0.8 mL of PBS W/Ca^{2+} and W/Mg^{2+}, then incubated in 400 μL of PFA 4% solution in PBS for 20 min at room temperature, and rinsed three times with fresh PBS before staining with DAPI (400 μL, 10.8 μg/mL, 20 min room temperature). The samples were left in PBS for confocal image acquisition using a Nikon ECLIPSE Ti inverted fluorescence microscope for super-resolution imaging, collecting multistack pictures by laser excitation at 561.6 and 405 nm and collecting fluorescence emission through 595/50 (Rhodamine) and 450/50 nm (DAPI) band-pass filters. Captured images were processed using Fiji software for semiquantitative analysis of fluorescence intensity of A431 WT or A431-CCK2-R$^+$ cells associated with IP-002$_x$-Rho compounds. RGB pictures were divided into blue and red channel subimages and converted into 32-bite gray types. The fluorescence intensity values for the red channel were extracted from 10 ROIs per image and

https://doi.org/10.1021/acs.molpharmaceut.4c00124
Mol. Pharmaceutics 2024, 21, 3848−3865

Scheme 2. Synthesis of Thiosaccharides. ***Reagents and Conditions*****: (a) Ac_2O, NaOAc, Reflux, 4 h, and 82−90% yield; (b) HBr 30% in CH_3COOH, CH_2Cl_2, Room Temperature, 30 min, and 75−100% Yield; (c) Thiourea, Acetone, Reflux, 3 h, and Quantitative Yield; (d) $Na_2S_2O_5$, H_2O, CH_2Cl_2, 100°C, 3.5 h, and 45−93% Yield; and (e) NaOMe, MeOH, Room Temperature, 16 h, DOWEX-H^+, and Quantitative Yield**

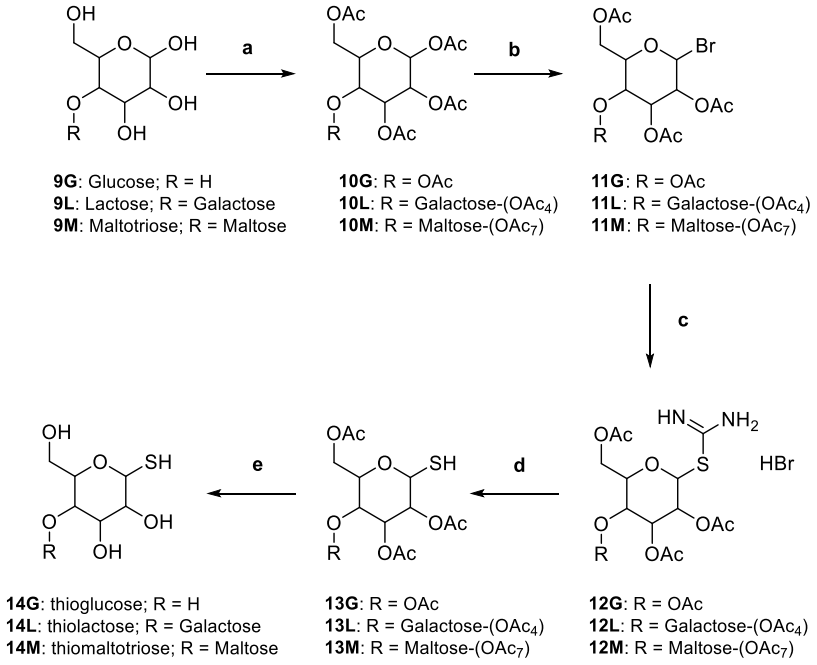

Scheme 3. Synthesis of IP-002$_x$-Rho. ***Reagent and Conditions*****: (a) TEA, Propionitrile, MeOH, 50°C, 48 h, and 15−30% Yield and (b) Pd/C 10%, H2, EtOH, 18h, Room Temperature, and 91% Yield**

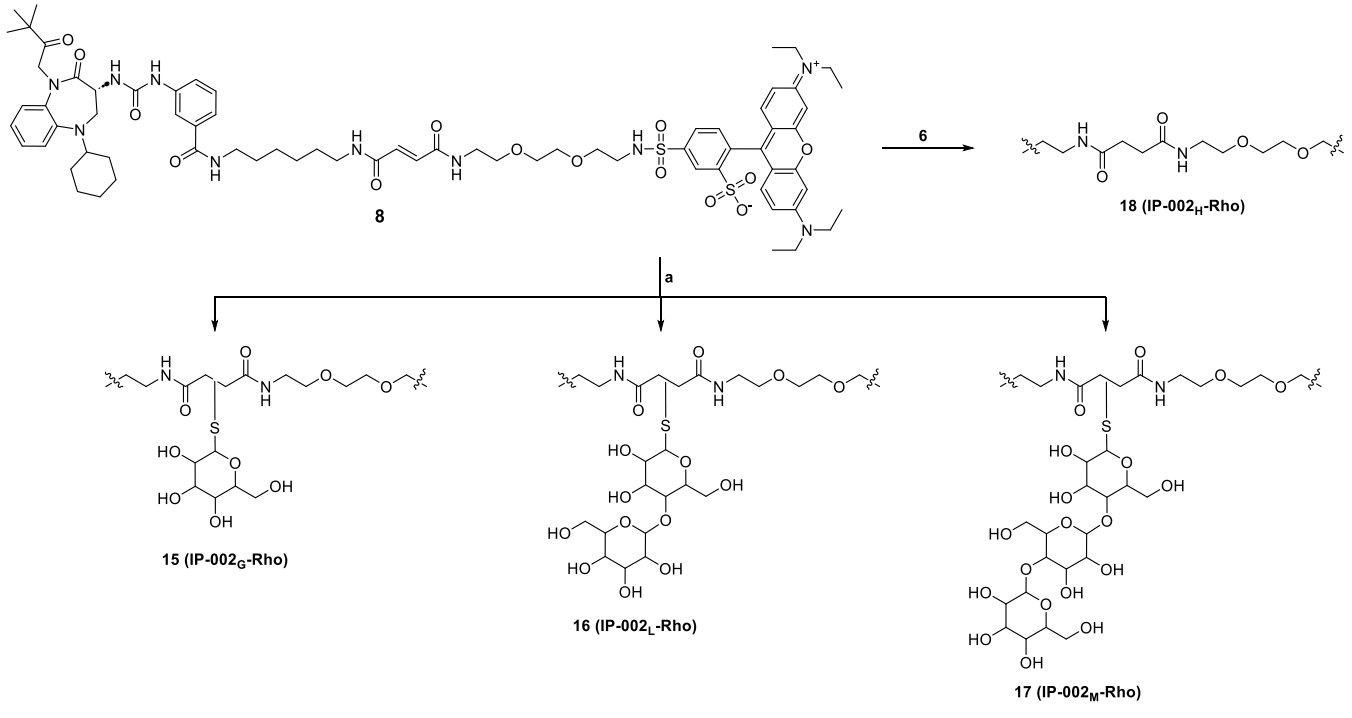

normalized to the pixel numbers. All data were expressed in arbitrary fluorescent units as the mean ± SD.

2.8.8. Statistical Analysis. All samples were prepared in triplicate, and data are shown as the mean ± standard deviation of two or three independent experiments. Statistical analysis was performed with GraphPad Prism software v9.2. Statistical significance was calculated using one-way or two-way analysis of variance (ANOVA) with Tukey post hoc comparisons, setting $p < 0.05$ as a level of significance.

3. RESULTS AND DISCUSSION

In this work, we propose a chemical modification of the nastorazepide-based SPECT tracer (i.e., IP-001) published by our group,[27] to reduce its hydrophobicity, which limits CCK2-

https://doi.org/10.1021/acs.molpharmaceut.4c00124
Mol. Pharmaceutics 2024, 21, 3848−3865

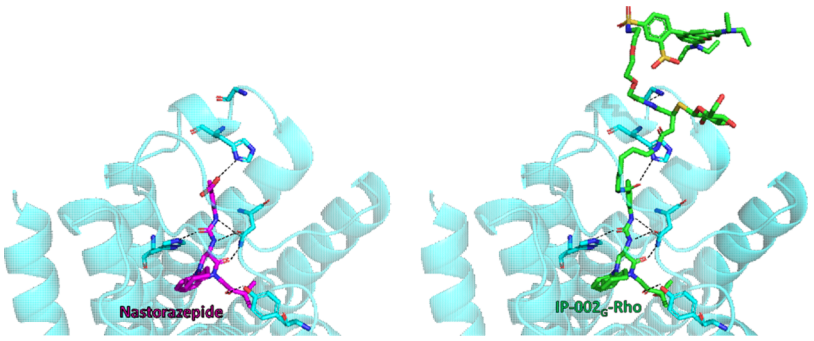

Figure 2. Binding mode predicted for nastorazepide (A) and **IP-002$_G$-Rho** (B) in CCK2-R. Residues involved in H-bonds with the ligands are shown in sticks. H-bonds are highlighted as dashed black lines.

R^+ cell-specific association and suboptimal biodistribution after in vivo administration. Therefore, we generated a small library of IP-002$_x$-Rho derivatives containing a pendant group of increasing hydrophilicity (H < glucose < lactose < maltotriose), as depicted in Figure 1.

3.1. Synthesis of IP-002$_x$-Rho. The fluorescent analogues of **IP-001** were synthesized by starting from a common intermediate (**8**, Scheme 1).

Briefly, the starting nastorazepide (**1**; synthesized according to the procedure reported by our group[17]) was condensed with *N*-Boc-1,6-hexandiamine to yield compound **2**, followed by selective BOC deprotection in acid conditions to yield **3**. The free terminal amino group of compound **3** was then coupled with synthon **5**, previously obtained by the HATU-mediated reaction between commercially available *N*-Boc-2,2′-(ethylenedioxy)diethylamine and maleic anhydride. The Boc protecting group of **6** was then removed by acid hydrolysis, yielding compound **7**, which was finally condensed with rhodamine B sulfonyl chloride to give functionalizable fluorescent intermediate **8**. Of note, the maleic moiety can be exploited for further reacting compound **8** either by hydrogenation or by using Michael donor reagents as thiosaccharides, thus obtaining the series of compounds with increasing hydrophilicity. The synthesis of thiosaccharides is reported in Scheme 2, whereas the synthesis of the final **IP-002$_X$-Rho** compounds is reported in Scheme 3.

The thiosaccharides were synthesized following the procedures reported by Floyd et al.[35] Briefly, the starting saccharide (either glucose, lactose, or maltotriose; **9G**, **9L**, and **9M**, respectively) was fully acetylated with acetic anhydride and sodium acetate to yield the derivatives **10G, L**, and **M**, respectively. Selective bromination at the anomeric carbon and subsequent condensation with thiourea yielded the thiouronic derivatives **12G**, **L**, and **M**, which were treated with sodium metabisulfite to obtain the reduced thiolic derivatives **13G, L**, and **M**, respectively. The acetyl groups were finally removed under strong alkaline conditions to yield the desired thiosaccharides **14G, L**, and **M**. Compounds **14G, L**, and **M** were unstable under atmospheric conditions, as the free thiolic functions tend to readily oxidize to disulfides. Accordingly, the synthesized thiosaccharides must be freshly prepared immediately before their use in the following reactions.

As mentioned before, compound **8** was either subjected to condensation with the thiosaccharides (yielding compounds **IP-002$_G$-Rho**, **IP-002$_L$-Rho**, and **IP-002$_M$-Rho**) or to catalytic hydrogenation (yielding compound **IP-002$_H$-Rho**). As shown in Scheme 3, the exact position of the condensation of the thiosaccharide to the conjugated double bond was not determined.

3.2. Molecular Modeling. Molecular docking studies with nastorazepide and **IP-002$_G$-Rho** and the very recently reported cryo-EM structure of CCK2-R[36] were preliminarily conducted to ascertain that the modification of the drug structure, and in particular the introduction of the saccharide pendants, did not affect the binding mode with the receptor. **IP-002$_G$-Rho** was selected as a model nastorazepide derivative with pendant sugar. As depicted in Figure 2, the compounds shared the same interactions with the CCK2-R. Indeed, both nastorazepide and **IP-002$_G$-Rho** were well inserted into the hydrophobic cavity of the receptor, establishing H-bonds with Tyr189, Asn353, His364, and His376. Moreover, the linker spacer of **IP-002$_G$-Rho** contributed an additional H-bond with the Gly362 backbone. Conversely, the glycosylated moiety of **IP-002$_G$-Rho** as well as the rhodamine pointed out from the receptor, confirming that the presence of hydrophilic pendants and the fluorophore may have no detrimental effects on the binding.

3.3. IP-002$_x$-Rho Solubility Tests. As shown in Table 1, the solubility of the synthesized **IP-002$_x$-Rho** derivatives in aqueous buffer mimicking the physiological conditions (i.e., PBS) was evaluated by RP-HPLC analysis. The collected data, together with the retention time (R_t) detected and the calculated cLogP, were considered predictive of the hydrophilic/hydrophobic behavior of the compound (Table 1). In **IP-002$_G$-Rho**, the insertion of a glucose unit improved only slightly the solubility in PBS with respect to **IP-002$_H$-Rho**. This might be caused by the highly lipophilic and rigid nature of both the targeting agent and the fluorophore, as described in systems containing rigid backbones and OEG-glucose combined moieties.[37] More flexible and hydrophilic residues such as lactose and maltotriose instead led to an improvement of the solubility of the compounds in aqueous media, as shown by the lower cLogP values obtained for **IP-002$_L$-Rho** and **IP-002$_M$-Rho** with respect to **IP-002$_H$-Rho** and **IP-002$_G$-Rho**. In

Table 1. Solubility (S) of IP-002$_x$-Rho Derivatives in Phosphate Buffer Saline (PBS) as Obtained by HPLC Measurements and cLogP Values

code	S (μg·mL^{-1})	cLogP[a]
IP-002$_H$-Rho	0.131 ± 0.113	12.97
IP-002$_G$-Rho	0.228 ± 0.027	10.20
IP-002$_L$-Rho	0.774 ± 0.096	8.03
IP-002$_M$-Rho	2.794 ± 0.249	5.85

[a]cLogP values were calculated with OpenBabel.[38]

https://doi.org/10.1021/acs.molpharmaceut.4c00124
Mol. Pharmaceutics 2024, 21, 3848−3865

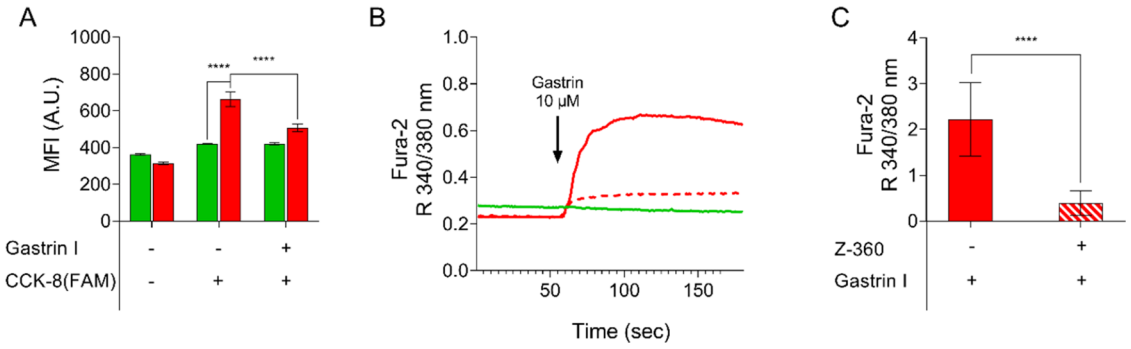

Figure 3. (A) CCK-8(FAM) association with A431 WT (green) and A431 CCK2-R$^+$ cells (red) after 30 min of incubation in the presence or absence of a large excess of gastrin I (MFI: mean fluorescence intensity). Values are expressed as the mean ± SD of three independent experiments performed in triplicate. (B) Traces of cytosolic Ca^{2+} measurements (expressed as Fura-2 340/380 nm ratio) in A431 WT (green full line) and A431-CCK2-R$^+$ (red full line) cells upon stimulation with 10 μM gastrin I. A431-CCK2-R$^+$ were additionally preincubated with Z-360 before stimulation with gastrin I (red dashed line). The reported traces are the average of n = 72−85 cells from three independent experiments. (C) Ca^{2+} response was fully blocked in 62% of A431-CCK2-R$^+$ cells by 2 min preincubation with 1 μM Z-360 before gastrin I addition and at least attenuated by a factor of 5 in the remaining positive cells (stripped bar).

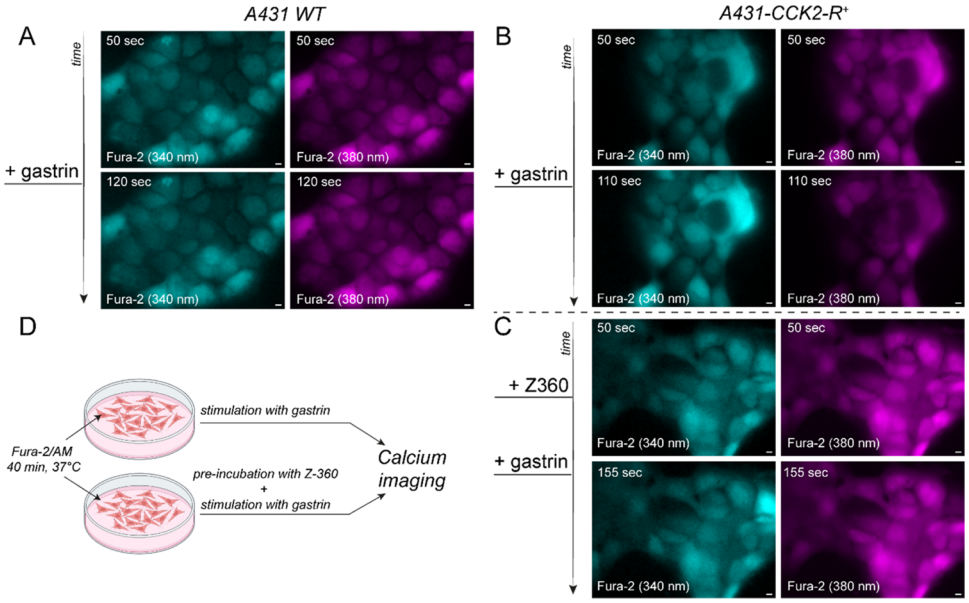

Figure 4. Representative images of calcium imaging with reporter Fura-2 AM. (A, B) Both A431 WT and A431-CCK2-R$^+$ cell lines were incubated with Fura-2-AM solution at 37 °C in the dark, and the fluorescence was recorded by exciting at 340 and 380 nm, before and upon addition of 10 μM Gastrin, as indicated. (C) Same experiment was repeated in A431-CCK2-R$^+$ cells preincubated for 2 min with 1 μM Z-360 before 10 μM gastrin I addition. (D) Schematic representation of the assay (created with Biorender.com). Scale bar: 10 μm.

particular, the presence of a maltotriose residue in **IP-002$_M$-Rho** resulted in at least a 10-fold increase in the compound solubility compared to IP-002$_G$-Rho, thus pointing out this molecule as the most promising candidate.

3.4. Cell Line Characterization: CCK2-R Expression. In our previous work,[27] we already screened the CCK2-R expression by several cell lines, highlighting that a basal expression could be observed in A431 cells. Here, via Western blot, we compared the receptor expression by A431 WT and A431 cells transfected to overexpress CCK2-R. Our results (Figure S1) supported the higher expression of the target receptor in the A431-CCK2-R$^+$ cell line, even though a basal level of receptor expression by the A431 WT was still observed.

We then further investigated the receptor expression level on the two cell lines (Figures S2 and S3) by monitoring the association with a natural ligand, such as the cholecystokinin-8 peptide (CCK-8).[39] CCK-8 labeled with aminofluoroescein (CCK-8(FAM)) was incubated for 30 min with both cell lines in the presence or absence of another natural ligand, gastrin I, that was used for competition studies. We observed a higher association of CCK8(FAM) with the CCK2-R$^+$-cell line as compared to the WT cells. Importantly, when A431-CCK2-R$^+$ cells were pretreated with an excess of gastrin I, a statistically significant (p < 0.0001, two-way ANOVA) decrease of CCK-8(FAM) association was observed (Figure 3A), although it was not possible to achieve a complete blockage of the association despite the large excess of gastrin I used. On the contrary, this effect was not detected for A431 WT cells, and in general, a lower ligand association was registered on this cell line as compared to A431-CCK2-R$^+$ cells. We hypothesized that the lipophilic nature of CCK8(FAM) might be responsible for the only partial blocking of the association with A431-CCK2-R$^+$ cells and of the internalization by simple diffusion observed in

https://doi.org/10.1021/acs.molpharmaceut.4c00124
Mol. Pharmaceutics 2024, 21, 3848−3865

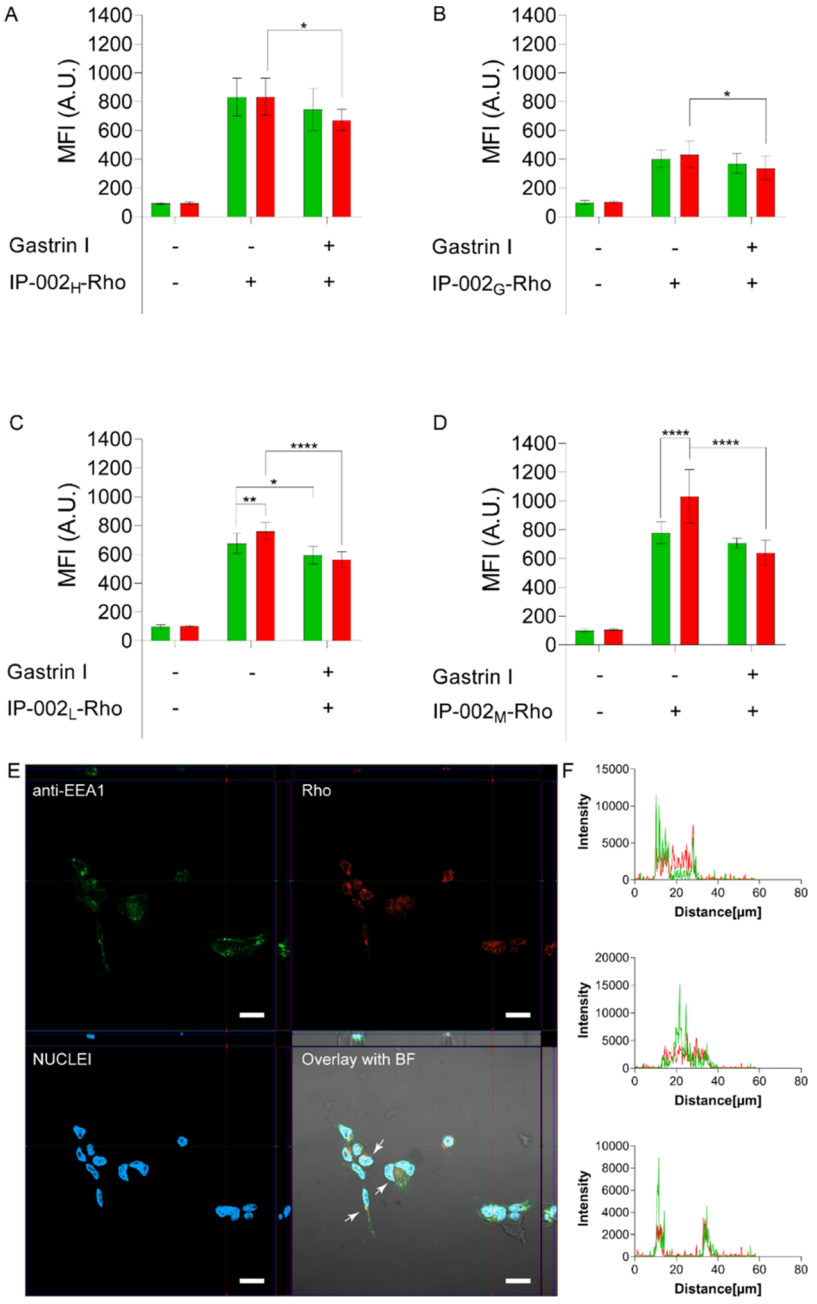

Figure 5. Association of (A) **IP-002$_H$-Rho**, (B) **IP-002$_G$-Rho**, (C) **IP-002$_L$-Rho, and** (D) **IP-002$_M$-Rho** with A431 WT (green bars) and A431-CCK2-R$^+$ (red bars) cell lines in the presence or absence of the natural ligand gastrin I (50 μg/mL) as assessed by flow cytometry (FC) analysis. Cells were exposed to 0.5 μg/mL IP-002$_x$-Rho, and the association was assessed after 30 min. MFI: mean fluorescence intensity. Values are expressed as the mean of three independent experiments ± SD (*= $p < 0.05$; **** = $p < 0.0001$). (E) Confocal laser scanning microscopy images for colocalization analysis. Orthogonal sections of A431-CCK2-R$^+$ cells after 1 h of incubation with the IP-002$_M$-Rho (red) and anti-EEA-1 antibody (green) from the maximum intensity projection images. Nuclei were visualized using Hoechst 33258. Scale bar: 20 μm. (F) Intensity profile graphs of IP-002$_M$-Rho (red) colocalization with EEA-1 (green). Line scan graphs showing the immunofluorescence intensity along the cells indicated by the positioned arrow in (E), "Overlay with BF".

the A431 WT line, as suggested by the lack of differences between the uptake and competition results.

Finally, to assess the membrane expression and coupling to G-proteins of the CCK-2 receptor, the intracellular Ca^{2+} release was measured. A431 WT cells did not show Ca^{2+} release in the presence of gastrin I or CCK-8 (Figures 3B and 4A), whereas both CCK-8 and gastrin I increased the Ca^{2+} release in ∼80% of the CCK2-R$^+$ cells, with similar responses induced by the two ligands (Figures 3B and 4B and S3BC and S4). Pretreatment of A431-CCK2-R$^+$ cells with 1 μM Z-360 solution in mKRB medium inhibited most gastrin I-induced intracellular Ca^{2+} release (Figures 3C and 4C), while Z-360 alone did not increase Ca^{2+} release as compared to the cell basal activity (Figure S3D). These results suggested that the CCK2-R expression was maintained in most transfected cells but not in the entire population, possibly due to a loss of CCK2-R encoding plasmid but not Geneticin resistance.

For A431 cells, Western blot analysis revealed the presence of the receptor (total cell lysates, Figure S1), while the calcium signaling assay did not show any positive signal after cell

https://doi.org/10.1021/acs.molpharmaceut.4c00124
Mol. Pharmaceutics 2024, 21, 3848−3865

stimulation with the CCK2R agonist or antagonist (Figures 3B and 4A). On the contrary, A431 WT cells responded to ATP stimulation, demonstrating that the machinery for inositol 1,4,5-trisphosphate production and subsequent intracellular Ca^{2+} release was functional (data not shown). Therefore, we postulated that either the receptor is intracellularly located or it is displayed at the cytoplasm membrane in an inactive form that is not coupled with G-proteins.

3.5. Investigation of IP-002x-Rho Cell Association and Internalization. The new compounds were tested in vitro for their selective association with the A431 WT and A431-CCK2-R^+ cells (Figures 5A and S5). **IP-002$_H$-Rho** showed a high fluorescence intensity in both A431 WT and A431-CCK2-R^+ cell lines with no differences between the two groups. Indeed, the ratio of the mean fluorescence intensity signal detected in A431 WT or A431 CCK2-R^+ cells was ca. 1.00, indicating a complete lack of selectivity toward CCK2-R-expressing cells. To evaluate whether the association was at least in part mediated by the specific receptor, competition experiments were performed by repeating the assay in the presence of an excess of the natural ligand gastrin I. While **IP-002$_H$-Rho** association with A431-CCK2-R^+ cells was slightly but significantly reduced by preincubation with gastrin I ($p < 0.001$), A431 WT cells showed comparable fluorescence independently of the presence of gastrin I. All together, these results suggested a remarkable **IP-002$_H$-Rho** association with both cell lines with a limited receptor-mediated internalization, likely due to the high lipophilicity of the compound. In fact, both Wayua et al. and Kaloudi et al. hinted at issues with the hydrophobic nature of the Z-360 targeting agent, which led to high background noise in in vivo biodistribution studies of conjugated radiotracers.[26,40] Although the insertion of a glucose unit in the spacer significantly reduced the cell association in both tested cell lines compared to **IP-002$_H$-Rho** (Figure 5B), likely due to a lower passive diffusion because of the higher hydrophilicity of the compound, **IP-002$_G$-Rho** did not improve the selectivity for the targeted cells in competition assays. Conversely, enhanced specific association with A431-CCK2-R^+ cells was observed for the compounds characterized by the insertion of a di- and trisaccharide in the spacer, with **IP-002$_M$-Rho** outperforming **IP-002$_L$-Rho** (Figure 5C,D). The ratio of the compound association with A431-CCK2-R^+ cells with respect to A431 WT cells was indeed increasing proportionally with its hydrophilicity, with 1.05(±0.10)-, 1.09(±0.09)-, 1.14-(±0.04)-, and 1.37-(±0.05)-fold increase for **IP-002$_H$-Rho**, **IP-002$_G$-Rho**, **IP-002$_L$-Rho**, and **IP-002$_M$-Rho**, respectively. The differences in the cell association observed between the two cell lines were also subjected to statistical analysis, which showed significance only for IP-002$_L$-Rho and IP-002$_M$-Rho compounds. Competition assays confirmed that **IP-002$_M$-Rho** was superior when compared to all the other tested derivatives, since the decrease of cell association obtained by preincubating A431-CCK2-R^+cells with gastrin I went from 19.8% when using **IP-002$_H$-Rho** to about 29% with both **IP-002$_G$-Rho** and **IP-002$_L$-Rho** and to 42.3% with **IP-002$_M$-Rho**. Similar results were obtained by performing competition studies with **IP-002$_H$-Rho** and **IP-002$_M$-Rho** compounds and using an equimolar concentration of Z-360 as an inhibitor (Figure S5). Moreover, the cell association results were in good agreement with the solubility test and the clogP values (Table 1). The progressive increase of the hydrophilicity going from **IP-002$_H$-Rho** to **IP-002$_M$-Rho** imparted receptor-specific recognition property only to the latter. However, a certain level of passive diffusion and probably macropinocytosis,[41] that is highly active in cancer cells, was always detectable at the concentration tested for all compounds.

IP-002$_M$-Rho with A431-CCK2-R^+cells was also investigated by a laser scanning confocal microscope, which showed that the red signal was largely confined to the cytoplasmatic compartment (Figure S6), where it seems to be partially diffused and partially entrapped in subcellular organelles.

Preliminary trafficking studies suggested a certain level of colocalization of the red signal due to the Rhodamine labeling of **IP-002$_M$-Rho** and the early endosome marker EEA-1, visualized in green (Figures 5E and S7 and S8). The calculated Pearson's coefficient for EEA-1 and **IP-002$_M$-Rho** colocalization was 0.339 ± 0.0975, indicating a moderate positive correlation, as also confirmed by the line scan graphs reported in Figure 5F showing an overlapping immunofluorescence for EEA-1 and **IP-002$_M$-Rho**. Altogether, our data seem to suggest that **IP-002$_M$-Rho** is not only bound to the receptor at the plasma membrane but also internalized after the binding. The internalization of CCK2-R antagonists has been thoroughly investigated in the last decades and was first reported by Roettger et al.[42,43] Although different synthetic antagonists did not induce receptor internalization,[44] benzodiazepine-like structures were found to promote this phenomenon. For instance, Akgün et al.[45] showed that the binding of specific antagonists causes a conformational change of CCK-2 receptors, which induces cellular internalization via β-arrestin-2 recruitment.[46] These findings could also be extended to cellular uptake phenomena observed in macromolecular systems exploiting CCK2-R antagonists as targeting agents, as recently described by Kaloudi et al.[25,40] and Nock et al.[47] Thus, we can postulate that there is a receptor-mediated mechanism contributing to **IP-002$_M$-Rho** internalization by cells, although further investigation is required. Of note, the efficient internalization of **IP-002$_M$-Rho** could be a favorable feature for developing receptor-targeted tumor radiotherapy by facilitating the accumulation of radioactivity close to the cell nucleus. This aspect could not only improve the efficacy of β^--emitters but also exploit the Auger electrons (i.e., more potent radiations with a short tissue penetration range) to improve the safety of the systems toward healthy tissues.[48]

3.6. GelMA Scaffold Characterization and Selection. The viscoelastic properties of 10, 16, 20, and 25% w/V GelMA revealed that all samples had a storage modulus (G') higher than the loss modulus (G''), as shown in Figure S9. Thus, all the tested conditions showed a predominantly elastic behavior rather than a viscous one. This was expected because the elastic-dominated behavior of GelMA hydrogels is due to the high degree of methacrylation (~70%) and is proof of effective photo-cross-linking. To quantify the mechanical properties of the hydrogels, the storage modulus of the different samples was considered since G' is an indicator of the elasticity of the material. There was a noticeable correlation between the amount of GelMA in the hydrogel and the storage modulus. In all hydrogels, the G' was constant in the temperature range tested (15−45 °C).

To maximize the radiopharmaceutical diffusion through the hydrogel matrix, which is crucial for its interaction with the embedded cells, together with the preservation of the shape and the stability of the construct when handled and in cell medium, a 16% GelMA concentration was selected as optimal and was used for the following studies.

https://doi.org/10.1021/acs.molpharmaceut.4c00124
Mol. Pharmaceutics 2024, 21, 3848−3865

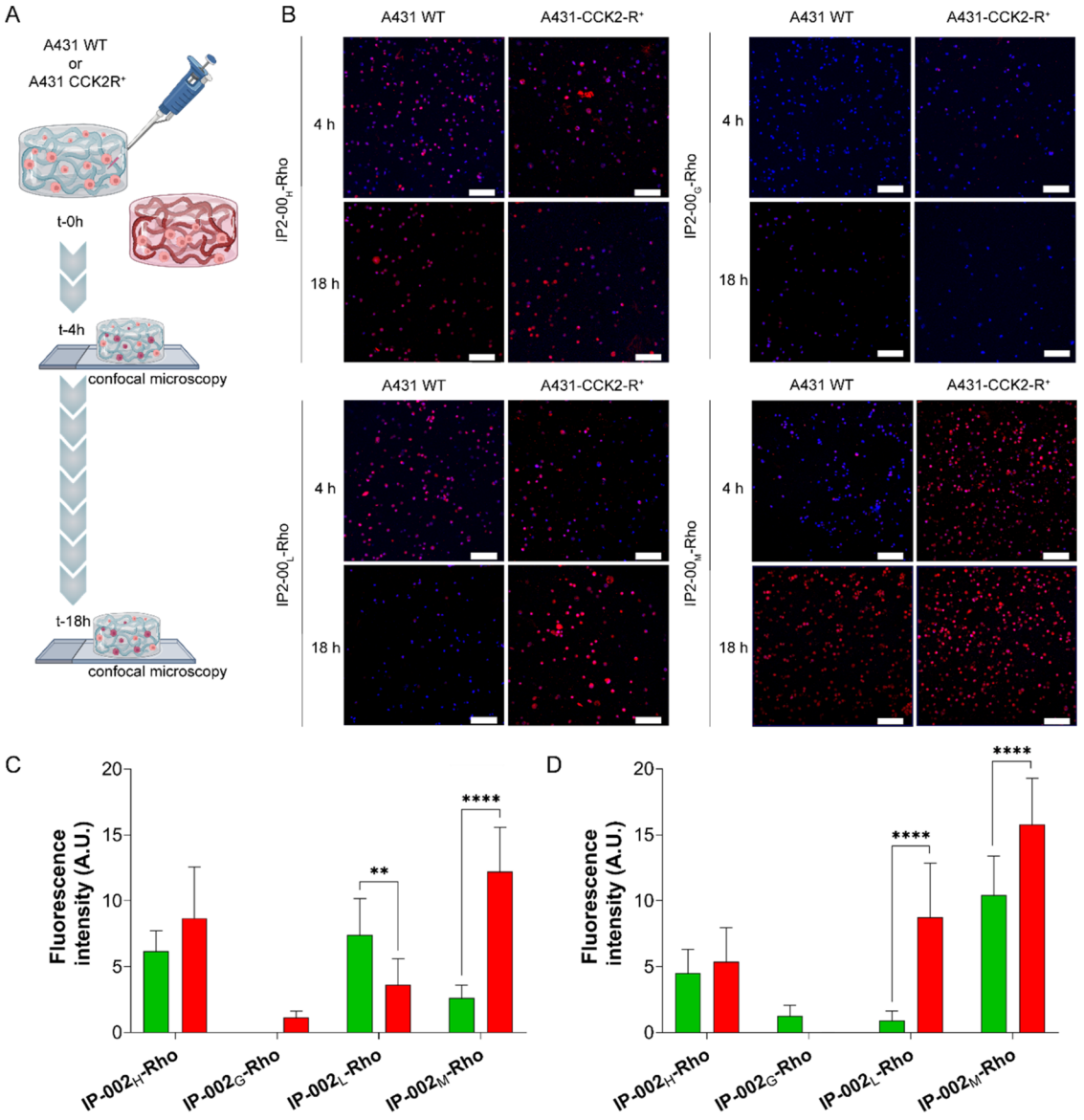

Figure 6. (A) Schematic representation of the assay (created with Biorender.com): A431 WT or A431-CCK2-R$^+$ cell-embedded scaffold (16% w/V GelMa) were incubated on day 4 with 25 μg/mL **IP-002$_x$-Rho** for 4 or 18 h at 37 °C. At each time point, the medium was removed and the scaffolds were extensively rinsed with PBS, fixed with 4% PFA, and after nuclei staining with DAPI were imaged by confocal microscopy. (B) Confocal microscopy images of the cell-embedded 3D scaffold incubated with **IP-002$_x$-Rho** for 4 or 18 h at 37 °C. Scale bar: 100 μm. (C, D) Semiquantitative analysis of fluorescence intensity of **IP-002$_x$-Rho** signals after 4 (C) or 18 (D) h of incubation with the A431 WT (green bars) or A431-CCK2-R$^+$ (red bars) cell-embedded scaffold.

3.7. IP-002$_x$-Rho Cell Association in a 3D Scaffold Model. The cell association of **IP-002$_x$-Rho** compounds was further assessed on 3D GelMA scaffolds with embedded WT A431 or A431-CCK2-R$^+$ cells. First, the viability of the encapsulated cells in 3D scaffolds was assessed by a Live/Dead cell imaging kit to evaluate whether the model was appropriate for cellular proliferation and tissue mimicking. As reported in Figure S10, more than 80% of the A431 WT and CCK2-R$^+$ embedded cells were viable (Figure S10, Calcein staining displayed in green) and homogeneously distributed within the gel structure, although a slightly higher cell death (Figure S10, Propidium Iodide staining displayed in red) could be appreciated in A431-CCK2-R$^+$-seeded scaffolds. These observations suggested that the size and porosity of the scaffolds were sufficient to guarantee the diffusion of nutrients and oxygen without causing cell hypoxia. From the micrographs, it was also possible to visualize much larger green spots, i.e., viable cells, than red spots (i.e., dead cells). This observation seems to suggest that viable cells associate in clusters, which correlates well with cell proliferation within the scaffold, thus confirming the environment's appropriateness for cell growth. Oregon Green-labeled phallodin was used to stain the cell cytoskeleton and check the cell morphology after being embedded in the scaffold. Both A431 WT and A431-CCK2-R$^+$ cells maintained the typical elongated morphology at day 4 after the embedding and GelMa cross-linking procedure (Figure S11), well in agreement with the good viability results observed with the Live/Dead staining. This analysis further validated the possibility of using the GelMA 3D scaffold to encapsulate cells and as a simple model to evaluate the compound−cell interaction in a three-dimensional environment.

https://doi.org/10.1021/acs.molpharmaceut.4c00124
Mol. Pharmaceutics 2024, 21, 3848−3865

Next, we used the A431 WT or A431-CCK2-R$^+$ cell-embedded scaffold to evaluate the compound interaction with cells in a 3D model (Figure 6). As schematized in Figure 6A, 4 days old scaffolds with embedded cells were incubated in IP-002$_x$-Rho-containing medium for 4 or 18 h and then imaged by confocal microscopy to evaluate both the diffusion of the compounds in a three-dimensional structure and the uptake by cells. Semiquantitative analysis of the fluorescence signals was carried out (Figure 6C,D). All compounds were observed to freely diffuse throughout the matrix, as demonstrated by the Rho-associated fluorescence intensity recorded in the core of the scaffold even after 4 h of incubation (Figure 6B,C, 4 h time point). Moreover, in **IP-002$_H$-Rho**- and **IP-002$_L$-Rho**-treated samples, it was possible to detect a similar association at 4 h incubation (i.e., rhodamine fluorescence signal). In **IP-002$_H$-Rho**-treated samples, the uptake was similar in both cell lines, while A431-CCK2-R$^+$ cells embedded in the GelMA scaffold seemed to internalize less **IP-002$_L$-Rho** in comparison to A431 WT cells, as suggested by the lower fluorescence intensity detectable. The trend was maintained for **IP-002$_H$-Rho**-treated samples after 18 h of incubation. Conversely, for **IP-002$_L$-Rho** at the 18 h time point, we observed a much higher uptake by A431-CCK2-R$^+$ as compared to A431 WT cells, where the fluorescence signal almost disappeared. **IP-002$_G$-Rho** showed negligible uptake in both cell lines and at both time points. The results confirmed **IP-002$_M$-Rho** as the best-performing derivative since in all conditions, a higher cell uptake was observed as compared to the other compounds, with superior selectivity toward A431-CCK2-R$^+$ with respect to A431 WT cells at both time points, even though the 4 h incubation time showed the best selectivity for the targeted cells. Of note, the high selectivity for A431-CCK2-R$^+$ cells showed by **IP-002$_L$-Rho** after 18 h of incubation indicates that this derivative, which bears a disaccharide substituent in the spacer, deserves further investigation.

4. CONCLUSIONS

In this study, we designed and generated a small library of CCK2-R-targeting compounds characterized by the presence of the substituent of increasing hydrophilicity (H < glucose < lactose < maltotriose) in the spacer linking Z-360, a CCK2-R-targeting agent, with a fluorescence probe, a Rhodamine derivative. The library represents a prototype of macromolecules where the fluorescent molecule, introduced here to facilitate the monitoring of the library interaction with cells in 2D and 3D in vitro models, could be replaced with a drug or a chelator to embed metal radionuclides for diagnostic and therapeutic purposes. Our previous studies showed that the highly hydrophobic nature of Z-360 might affect the in vitro and in vivo behavior of its derivatives, thus limiting cell-specific recognition and in vivo efficacy. Here, we aimed at identifying the minimal structural requirements to ensure a cell-specific association. Hence, solubility, association, and competition assays were performed in 2D in vitro models using A431 WT (CC2-R-underexpressing cells) or A431-CCK2-R$^+$ (CCK2-R-overexpressing cells) cell lines. The solubility tests in PBS indicated that there is a linear correlation between this parameter, the calculated logP values, and the sugar molecular size, with the monosaccharide derivative (**IP-002$_G$-Rho**, solubility of 0.228 μg/mL, logP 10.20) being the less soluble and the trisaccharide-bearing derivative being the most soluble (**IP-002$_M$-Rho**, solubility of 2.794 μg/mL, logP 5.85). **IP-002$_H$-Rho** which lacks a sugar residue was found to have the lowest solubility in PBS (0.131 μg/mL), well in agreement with the higher logP value. These findings correlate well with what was ascertained in the cellular uptake studies, where higher cell association was observed in both cell lines with **IP-002$_H$-Rho** and **IP-002$_M$-Rho**, which are the most lipophilic and soluble compounds, respectively. However, the hydrophobic nature of **IP-002$_H$-Rho** prevented cell-specific recognition, while **IP-002$_M$-Rho** showed a certain level of receptor-mediated endocytosis in both uptake (1.37-fold higher association with A431-CCK2-R$^+$ cells with respect to the A431 WT) and competition studies (42.3% blocking of the uptake in A431-CCK2-R$^+$ cells in the presence of the competitive ligand gastrin I). Finally, cell association in a complex tridimensional matrix made of GelMa confirmed optimal diffusion properties of all tested compounds within the entire thickness of the cylindrical scaffolds and improved association with CCK2-R-overexpressing cells in the case of **IP-002$_M$-Rho**, with high specificity at least at 4 h of incubation. Thus, **IP-002$_M$-Rho** has been pointed out as the best candidate for further structural modification suitable for the insertion of diagnostic and therapeutic radionuclides, propelling applications such as (radio)pharmaceuticals in diagnostics and therapeutics.

■ ASSOCIATED CONTENT

Supporting Information

The Supporting Information is available free of charge at https://pubs.acs.org/doi/10.1021/acs.molpharmaceut.4c00124.

> Western blot analysis for CCK2-R in A431 WT and A431-CCK2-R$^+$ cell lines; mean fluorescence intensity (MFI) from FC analysis of A431 WT and A431-CCK2-R$^+$ cell lines after 30 min of incubation with 5 μg/mL CCK-8(FAM) or 0.5 μg/mL IP-002$_H$-Rho; representative traces of cytosolic Ca^{2+} measurements in A431 WT and A431-CCK2-R$^+$ cells; representative images of Fura-2 AM calcium imaging; additional confocal laser scanning microscopy images of A431-CCK2-R$^+$ cells incubated with IP-002$_M$-Rho; temperature dependence of the storage modulus and loss modulus; and confocal microscopy images and analysis of A431 WT and A431-CCK2-R$^+$ cell morphologies after Oregon Green 488 phalloidin staining within the 3D scaffolds (PDF)

■ AUTHOR INFORMATION

Corresponding Authors

Giovanni Marzaro − *Department of Pharmaceutical and Pharmacological Sciences, University of Padova, 35131 Padova, Italy*; orcid.org/0000-0002-5892-5992; Email: giovanni.marzaro@unipd.it

Francesca Mastrotto − *Department of Pharmaceutical and Pharmacological Sciences, University of Padova, 35131 Padova, Italy*; orcid.org/0000-0002-2499-5490; Email: francesca.mastrotto@unipd.it

Authors

Elisa Vettorato − *Department of Pharmaceutical and Pharmacological Sciences, University of Padova, 35131 Padova, Italy; Legnaro National Laboratories, Italian Institute of Nuclear Physics (INFN), 35020 Legnaro (Padova), Italy*

https://doi.org/10.1021/acs.molpharmaceut.4c00124
Mol. Pharmaceutics 2024, 21, 3848−3865

Marco Verona − *Department of Pharmaceutical and Pharmacological Sciences, University of Padova, 35131 Padova, Italy*
Greta Bellio − *Department of Pharmaceutical and Pharmacological Sciences, University of Padova, 35131 Padova, Italy*
Stefania Croci − *Clinical Immunology, Allergy, and Advanced Biotechnologies Unit, AUSL-IRCCS of Reggio Emilia, 42122 Reggio Emilia, Italy*
Riccardo Filadi − *Department of Biomedical Sciences, University of Padova, 35131 Padova, Italy; Neuroscience Institute, National Research Council (CNR), 35131 Padua, Italy*
Alessandra Bisio − *Department of Cellular, Computational and Integrative Biology (CIBIO), University of Trento, 38123 Trento, Italy*
Eugenia Spessot − *Department of Industrial Engineering and BIOtech Research Center, University of Trento, 38123 Trento, Italy;* orcid.org/0000-0002-8367-7847
Alberto Andrighetto − *Legnaro National Laboratories, Italian Institute of Nuclear Physics (INFN), 35020 Legnaro (Padova), Italy*
Devid Maniglio − *Department of Industrial Engineering and BIOtech Research Center, University of Trento, 38123 Trento, Italy;* orcid.org/0000-0002-1653-861X
Mattia Asti − *Radiopharmaceutical Chemistry Section, Nuclear Medicine Unit, AUSL-IRCCS of Reggio Emilia, 42122 Reggio Emilia, Italy*

Complete contact information is available at: https://pubs.acs.org/10.1021/acs.molpharmaceut.4c00124

Author Contributions

E.V. and M.V.: methodology, validation, investigation, formal analysis, data curation, and writing—original draft preparation; G.B.: methodology, formal analysis, and writing—review and editing; S.C., R.F., A.B., E.S., D.M., and M.A.: investigation, formal analysis, and writing—review and editing; A.A.: funding acquisition; and F.M and G.M.: conceptualization, methodology, resources, data curation, supervision, writing—original draft preparation, review and editing, project administration, and funding acquisition. All authors have read and agreed to the published version of the article.

Author Contributions

◆E.V. and M.V. contributed equally to this work.

Funding

This research was funded by the Legnaro National Laboratories of the Italian Institute of Nuclear Physics ("ISOLPHARM_EIRA Project").

Notes

The authors declare no competing financial interest.

■ ACKNOWLEDGMENTS

The authors want to thank Dr Andrea Pagetta for his support with confocal image acquisition.

■ ABBREVIATIONS

6-FAM, 6-carboxyfluorescein; A431-CCK2R+, cell line A431 transfected to stably express CCK2R on the membrane; A431 WT, cell line A431 wild type; BSA, bovine serum albumin; CCK, cholecystokinin; CCK-8, cholecystokinin octapeptide; CCK-8(FAM), cholecystokinin octapeptide conjugated to 6-carboxyfluorescein; CCK2R, CCKB, CCK type 2 receptor; CH, cyclohexane; DAPI, 4′,6-diamidino-2-phenylindole dihydrochloride; DI, deionized (water); DMEM, Dulbecco's modified Eagle medium; DMF, dimethylformamide; DMSO, dimethyl sulfoxide; DOTA, 2,2′,2″,2‴-(1,4,7,10-tetraazacyclododecane-1,4,7,10-tetrayl)tetraacetic acid, tetraxetan; ECL, enhanced chemiluminescence; EDC, 1-ethyl-3-(3-(dimethylamino)propyl)carbodiimide; EDTA, ethylenediamine tetraacetic acid; EEA-1, early endosome antigen 1; EtOAc, ethyl acetate; FBS, fetal bovine serum; FC, flow cytometry; G-418S, Geneticin sulfate; GAPDH, glyceraldehyde-3-phosphate dehydrogenase; GelMA, methacryloyl gelatin; HATU, hexafluorophosphate azabenzotriazole tetramethyl uronium; HEPES, *N*-2-hydroxyethylpiperazine-*N*-2-ethanesulfonic acid; HPLC, high-performance liquid chromatography; HRMS, high resolution mass spectrometry; HRP, horseradish peroxidase; IgG, immunoglobulin G; IP-001, nastorazepide-based SPECT tracer; IP-002 nastorazepide-based IP-001 analogue proposed in this work; IP-002$_G$-Rho, IP-002 tracer conjugated with sulforhodamine B bearing a glucose residue; IP-002$_H$-Rho, IP-002 tracer conjugated with sulforhodamine B without a glucidic residue; IP-002$_L$-Rho, IP-002 tracer conjugated with sulforhodamine B bearing a lactose residue; IP-002$_M$-Rho, IP-002 tracer conjugated with sulforhodamine B bearing a maltotriose residue; IP-002$_X$-Rho, generic IP-002 tracer conjugated with sulforhodamine B; LAP, lithium phenyl-2,4,6-trimethylbenzoylphosphinate; MALDI TOF/TOF, matrix-assisted laser desorption/coupled ionization time of flight; MeCN, acetonitrile; MeOH, methanol; MG, minigastrin; mKRB, modified Krebs−Ringer bicarbonate; MOPS, 3-(*N*-morpholino)propanesulfonic acid; MWCO, molecular weight cutoff; MFI, mean fluorescence intensity; NMR, nuclear magnetic resonance; PBS, phosphate-buffered saline; PFA, paraformaldehyde; PI, propidium iodide; PRRT, peptide receptor radiotherapy; Rho, sulforhodamine B; PVDF, polyvinylidene fluoride; RIPA, radioimmuno-precipitation assay buffer; RIT, radio-immunotherapy; SD, standard deviation; SDS, sodium dodecyl sulfate; SPECT, single-photon emission computed tomography; TBS, tris-buffered saline; TEA, triethylamine; TFA, trifluoroacetic acid; TLC, thin-layer chromatography; YF460, netazepide; Z-360, nastorazepide

■ REFERENCES

(1) Roy, J.; Putt, K. S.; Coppola, D.; Leon, M. E.; Khalil, F. K.; Centeno, B. A.; Clark, N.; Stark, V. E.; Morse, D. L.; Low, P. S. Assessment of cholecystokinin 2 receptor (CCK2R) in neoplastic tissue. *Oncotarget* **2016**, *7* (12), 14605−14615.
(2) Zeng, Q.; Ou, L.; Wang, W.; Guo, D.-Y. Gastrin, Cholecystokinin, Signaling, and Biological Activities in Cellular Processes. *Front. Endocrinol.* **2020**, *11*, No. 112.
(3) Reubi, J. C.; Waser, B. Unespected High Incidence Of Cholecystokinin-B/Gastrin Receptors In Human Medullary Thyroid Carcinomas. *Int. J. Cancer* **1996**, *67*, 644−647.
(4) Smith, J. P.; Verderame, M. F.; McLaughlin, P.; Martenis, M.; Ballard, E.; Zagon, I. S. Characterization of the CCK-C (cancer) receptor in human pancreatic cancer. *Int. J. Mol. Med.* **2002**, *10*, 689−694.
(5) Dockray, G. J.; Moore, A.; Varro, A.; Pritchard, D. M. Gastrin Receptor Pharmacology. *Curr. Gastroenterol. Rep.* **2012**, *14*, 453−459.
(6) Roosenburg, S.; Laverman, P.; Joosten, L.; Eek, A.; Rutjes, F. P. J. T.; van Delft, F. L.; Boerman, O. C. In Vitro and In Vivo Characterization of Three 68 Ga- and 111 In-Labeled Peptides for Cholecystokinin Receptor Imaging. *Mol. Imaging* **2012**, *11*, No. 7290.2012.00001.
(7) Willard, M. D.; Lajiness, M. E.; Wulur, I. H.; Feng, B.; Swearingen, M. L.; Uhlik, M. T.; Kinzler, K. W.; Velculescu, V. E.;

Sjöblom, T.; Markowitz, S. D.; et al. Somatic mutations in CCK2R alter receptor activity that promote oncogenic phenotypes. *Mol. Cancer Res.* **2012**, *10*, 739−749.
(8) Mjønes, P.; Nordrum, I. S.; Sordal, O.; Sagatun, L.; Fossmark, R.; Sandvik, A.; Waldum, H. L. Expression of the Cholecystokinin-B Receptor in Neoplastic Gastric Cells. *Horm. Cancer* **2018**, *9* (1), 40−54.
(9) Cheal, S. M.; Sebastian, K. C.; Brett, A. V.; Nai-Kong, V. C.; Steven, M. L. Pretargeting: A Path Forward for Radioimmunotherapy. *J. Nucl. Med.* **2022**, *63* (9), 1302.
(10) Kraeber-Bodéré, F.; Bodet-Milin, C.; Rousseau, C.; Eugène, T.; Pallardy, A.; Frampas, E.; Carlier, T.; Ferrer, L.; Gaschet, J.; Davodeau, F.; et al. Radioimmunoconjugates for the Treatment of Cancer. *Semin. Oncol.* **2014**, *41* (5), 613−622.
(11) Bourgeois, M.; Bailly, C.; Frindel, M.; Guerard, F.; Chérel, M.; Faivre-Chauvet, A.; Kraeber-Bodéré, F.; Bodet-Milin, C. Radioimmunoconjugates for treating cancer: recent advances and current opportunities. *Expert Opin. Biol. Ther.* **2017**, *17* (7), 813−819.
(12) Camus, B.; Cottereau, A. S.; Palmieri, L. J.; Dermine, S. Indications of Peptide Receptor Radionuclide Therapy (PRRT) in Gastroenteropancreatic and Pulmonary Neuroendocrine Tumors: An Updated Review. *J. Clin. Med.* **2021**, *10* (6), No. 1267.
(13) Lu, X.; Lu, C.; Yang, Y.; Shi, X.; Wang, H.; Yang, N.; Yang, K.; Zhang, X. Current Status and Trends in Peptide Receptor Radionuclide Therapy in the Past 20 Years (2000−2019): A Bibliometric Study. *Front. Pharmacol.* **2021**, *12*, No. 624534.
(14) Mondello, P.; Cuzzocrea, S.; Navarra, M.; Mian, M. 90 Y-ibritumomab tiuxetan: a nearly forgotten opportunityr. *Oncotarget* **2016**, *7* (7), 7597−7609.
(15) Caplin, M. The recent European approval of lutetium (^{177}Lu) oxodotreotide increases treatment options for gastroenteropancreatic neuroendocrine tumors. *Int. J. Endocr. Oncol.* **2018**, *5* (2), No. IJE09.
(16) Fallah, J.; Agrawal, S.; Gittleman, H.; et al. FDA Approval Summary: Lutetium Lu 177 Vipivotide Tetraxetan for Patients with Metastatic Castration-Resistant Prostate Cancer. *Clin. Cancer Res.* **2023**, *29* (9), 1651−1657.
(17) Sgouros, G.; Bodei, L.; McDevitt, M. R.; Nedrow, J. R. Radiopharmaceutical therapy in cancer: clinical advances and challenges. *Nat. Rev. Drug Discovery* **2020**, *19* (9), 589−608.
(18) Knapp, F. F.; Dash, A. *Radiopharmaceuticals for Therapy*; Springer: New Delhi, 2016.
(19) Kue, C. S.; Kamkaew, A.; Burgess, K.; Kiew, L. V.; Chung, L. Y.; Lee, H. B. Small Molecules for Active Targeting in Cancer. *Med. Res. Rev.* **2016**, *36*, 494−575.
(20) Rottenburger, C.; Nicolas, G. P.; McDougall, L.; Kaul, F.; Cachovan, M.; Vija, A. H.; Schibli, R.; Geistlich, S.; Schumann, A.; Rau, T.; et al. Cholecystokinin 2 Receptor Agonist (177)Lu-PP-F11N for Radionuclide Therapy of Medullary Thyroid Carcinoma: Results of the Lumed Phase 0a Study. *J. Nucl. Med.* **2020**, *61* (4), 520−526.
(21) Klingler, M.; Hörmann, A. A.; Guggenberg, E. V. Cholecystokinin-2 Receptor Targeting with Radiolabeled Peptides: Current Status and Future Directions. *Curr. Med. Chem.* **2020**, *27* (41), 7112−7132.
(22) Ubl, P.; Gincu, T.; Keilani, M.; Ponhold, L.; Crevenna, R.; Niederle, B.; Hacker, M.; Li, S. Comparison of side effects of pentagastrin test and calcium stimulation test in patients with increased basal calcitonin concentration: the gender-specific differences. *Endocrine* **2014**, *46*, 549−553.
(23) Novak, D.; Anderluh, M.; Peitl, P. K. CCK(2)R antagonists: from SAR to clinical trials. *Drug Discovery Today* **2020**, *25* (8), 1322−1336.
(24) von Guggenberg, E.; Kolenc, P.; Rottenburger, C.; Mikołajczak, R. Update on Preclinical Development and Clinical Translation of Cholecystokinin-2 Receptor Targeting Radiopharmaceuticals. *Cancers* **2021**, *13* (22), No. 5776.
(25) Kaloudi, A.; Kanellopoulos, P.; Radolf, T.; Chepurny, O. G.; Rouchota, M.; Loudos, G.; Andreae, F.; Holz, G. G.; Nock, B. A.; Maina, T. [(99m)Tc]Tc-DGA1, a Promising CCK(2)R-Antagonist-Based Tracer for Tumor Diagnosis with Single-Photon Emission Computed Tomography. *Mol. Pharmaceutics* **2020**, *17* (8), 3116−3128.
(26) Wayua, C.; Low, P. S. Evaluation of a nonpeptidic ligand for imaging of cholecystokinin 2 receptor-expressing cancers. *J. Nucl. Med.* **2015**, *56*, 113−119.
(27) Verona, M.; Rubagotti, S.; Croci, S.; Sarpaki, S.; Borgna, F.; Tosato, M.; Vettorato, E.; Marzaro, G.; Mastrotto, F.; Asti, M. Preliminary study of a 1,5-benzodiazepine-derivative labelled with indium-111 for CCK-2 receptor targeting. *Molecules* **2021**, *26* (4), No. 918.
(28) Novak, D.; Tomašič, T.; Krošelj, M.; Javornik, U.; Plavec, J.; Anderluh, M.; Kolenc Peitl, P. Radiolabelled CCK2R Antagonists Containing PEG Linkers: Design, Synthesis and Evaluation. *ChemMedChem* **2021**, *16*, 155−163.
(29) Chen, B.-M.; Cheng, T.-L.; Roffler, S. R. Polyethylene Glycol Immunogenicity: Theoretical, Clinical, and Practical Aspects of Anti-Polyethylene Glycol Antibodies. *ACS Nano* **2021**, *15* (9), 14022−14048.
(30) Hoarau-Véchot, J.; Rafii, A.; Touboul, C.; Pasquier, J. Halfway between 2D and animal models: Are 3D cultures the ideal tool to study cancer-microenvironment interactions? *Int. J. Mol. Sci.* **2018**, *19*, 181.
(31) Weng, Q.; Zhou, L.; Xia, L.; Zheng, Y.; Zhang, X.; Li, F.; Li, Q. In vitro evaluation of FL118 and 9-Q20 cytotoxicity and cellular uptake in 2D and 3D different cell models. *Cancer Chemother. Pharmacol.* **2019**, *84*, 527−537.
(32) Low, P. S.; Wayua, C. Cholecystokinin B Receptor Targeting for Imaging and Therapy. U.S. Patent US 10080805 B2, 2018.
(33) Ren, T.; Grosshäuser, B.; Sridhar, K.; Nieland, T. J. F.; Tocchio, A.; Schepers, U.; Demirci, U. 3-D geometry and irregular connectivity dictate neuronal firing in frequency domain and synchronization. *Biomaterials* **2019**, *197*, 171−181.
(34) Aloj, L.; Caracò, C.; Panico, M.; Zannetti, A.; Del Vecchio, S.; Tesauro, D.; De Luca, S.; Arra, C.; Pedone, C.; Morelli, G.; et al. In vitro and in vivo evaluation of 111In-DTPAGlu-G-CCK8 for cholecystokinin-b receptor imaging. *J. Nucl. Med.* **2004**, *45*, 485−494.
(35) Floyd, N.; Vijayakrishnan, B.; Koeppe, J. R.; Davis, B. G. Thiyl Glycosylation of Olefinic Proteins: S-Linked Glycoconjugate Synthesis. *Angew. Chem., Int. Ed.* **2009**, *48*, 7798−7802.
(36) Zhang, X.; He, C.; Wang, M.; Zhou, Q.; Yang, D.; Zhu, Y.; Feng, W.; Zhang, H.; Dai, A.; Chu, X.; et al. Structures of the human cholecystokinin receptors bound to agonists and antagonists. *Nat. Chem. Biol.* **2021**, *17* (12), 1230−1237.
(37) Xue, C.; Velayudham, S.; Johnson, S.; Saha, R.; Smith, A.; Brewer, W.; Murthy, P.; Bagley, S. T.; Liu, H. Highly water-soluble, fluorescent, conjugated fluorene-based glycopolymers with poly-(ethylene glycol)-tethered spacers for sensitive detection of *Escherichia coli*. *Chem. - Eur. J.* **2009**, *15*, 2289−2295.
(38) O'Boyle, N. M.; Banck, M.; James, C. A.; Morley, C.; Vandermeersch, T.; Hutchison, G. R. Open Babel: An open chemical toolbox. *J. Cheminf.* **2011**, *3* (1), No. 33.
(39) Tirassa, P.; Manni, L.; Aloe, L.; Lundeberg, T. Cholecystokinin-8 and nerve growth factor: two endogenous molecules working for the upkeep and repair of the nervous system. *Curr. Drug Targets: CNS Neurol. Disord.* **2002**, *1* (5), 495−510.
(40) Kaloudi, A.; Kanellopoulos, P.; Radolf, T.; Chepurny, O. G.; Rouchota, M.; Loudos, G.; Andreae, F.; Holz, G. G.; Nock, B. A.; Maina, T. Tc-DGA1, a Promising CCK2R-Antagonist-Based Tracer for Tumor Diagnosis with Single-Photon Emission Computed Tomography. *Mol. Pharmaceutics* **2020**, *17*, 3116−3128.
(41) Palm, W. Metabolic functions of macropinocytosis. *Philos. Trans. R. Soc., B* **2019**, *374* (1765), No. 20180285.
(42) Roettger, B. F.; Rentsch, R. U.; Pinon, D.; Holicky, E.; Hadac, E.; Larkin, J. M.; Miller, L. J. Dual pathways of internalization of the cholecystokinin receptor. *J. Cell Biol.* **1995**, *128*, 1029−1041.
(43) Roettger, B. F.; Ghanekar, D.; Rao, R.; Toledo, C.; Yingling, J.; Pinon, D.; Miller, L. J. Antagonist-stimulated internalization of the G protein-coupled cholecystokinin receptor. *Mol. Pharmacol.* **1997**, *51*, 357−362.

https://doi.org/10.1021/acs.molpharmaceut.4c00124
Mol. Pharmaceutics 2024, 21, 3848−3865

(44) Magnan, R.; Masri, B.; Escrieut, C.; Foucaud, M.; Cordelier, P.; Fourmy, D. Regulation of membrane cholecystokinin-2 receptor by agonists enables classification of partial agonists as biased agonists. *J. Biol. Chem.* **2011**, *286*, 6707−6719.
(45) Akgün, E.; Körner, M.; Gao, F.; Harikumar, K. G.; Waser, B.; Reubi, J. C.; Portoghese, P. S.; Miller, L. J. Synthesis and in vitro characterization of radioiodinatable benzodiazepines selective for type 1 and Type 2 cholecystokinin receptors. *J. Med. Chem.* **2009**, *52*, 2138−2147.
(46) Magnan, R.; Escrieut, C.; Gigoux, V.; De, K.; Clerc, P.; Niu, F.; Azema, J.; Masri, B.; Cordomi, A.; Baltas, M.; et al. Distinct CCK-2 receptor conformations associated with β-arrestin-2 recruitment or phospholipase-C activation revealed by a biased antagonist. *J. Am. Chem. Soc.* **2013**, *135*, 2560−2573.
(47) Nock, B. A.; Kanellopoulos, P.; Chepurny, O. G.; Rouchota, M.; Loudos, G.; Holz, G. G.; Krenning, E. P.; Maina, T. Nonpeptidic Z360-Analogs Tagged with Trivalent Radiometals as Anti-CCK2R Cancer Theranostic Agents: A Preclinical Study. *Pharmaceutics* **2022**, *14*, No. 666.
(48) Ku, A.; Facca, V. J.; Cai, Z.; Reilly, R. M. Auger electrons for cancer therapy—a review. *EJNMMI Radiopharmacy Chem.* **2019**, *4* (1), No. 27.

https://doi.org/10.1021/acs.molpharmaceut.4c00124
Mol. Pharmaceutics 2024, 21, 3848−3865